Title

Derivation of Human Trophoblast Stem Cells from Pluripotent Stem Cells to Model Early Placental Development.

Journal

REPRODUCTIVE SCIENCES, 28(SUPPL 1)

ISSN

1933-7191

Authors

Soncin, Francesca
Horii, Mariko
Morey, Rob
et al.

Publication Date

2021

Peer reviewed

Derivation of functional trophoblast stem cells from primed human pluripotent stem cells

Francesca Soncin,[1,2*] Robert Morey,[2,3*] Tony Bui,[1,2] Daniela F. Requena,[1,2] Virginia Chu Cheung,[1,2,3] Sampada Kallol,[1,2] Ryan Kittle,[1,2] Madeline G. Jackson,[1,2] Omar Farah,[1,2] Jennifer Dumdie,[1,2] Morgan Meads,[1,2] Donald Pizzo,[1] Mariko Horii,[1,2] Kathleen M. Fisch,[3] Mana M Parast[1,2**]

[1]Department of Pathology, University of California San Diego, La Jolla, CA 92093, USA

[2]Sanford Consortium for Regenerative Medicine, University of California San Diego, La Jolla, CA 92093, USA

[3]Department of Obstetrics, Gynecology, and Reproductive Sciences, University of California San Diego, La Jolla, CA 92093, USA

*These authors contributed equally

**Correspondence: mparast@ucsd.edu

Summary

Trophoblast stem cells (TSC) have recently been derived from human embryos, and early first trimester placenta; however, aside from ethical challenges, the unknown disease potential of these cells limits their scientific utility. We have previously established a BMP4-based two-step protocol for differentiation of primed human pluripotent stem cells (hPSC) into functional trophoblast; however, those trophoblast could not be maintained in a self-renewing TSC-like state. Here, we use the first step from this protocol, followed by a switch to a newly-developed TSC media, to derive bona-fide TSC. We show that these cells resemble placenta- and naïve hPSC-derived TSC, based on their transcriptome, as well as *in vitro* and *in vivo* differentiation potential. We conclude that primed hPSC can be used to generate functional TSC, through a simple protocol which can be applied to a widely-available set of existing hPSC, including induced pluripotent stem cells, derived from patients with known birth outcomes.

Introduction

The human placenta is a unique transient organ, responsible for proper growth and development of the fetus in utero (Burton and Jauniaux, 2015). The epithelial cells in the placenta arise from trophectoderm (TE), the first lineage to segregate during embryonic development (Niakan et al., 2012). Much of what we know about trophoblast lineage specification and early placental development comes from studies in rodents; however, numerous studies using human embryos and early gestation placental tissues over the past few years have highlighted multiple key differences in these processes in human (Blakeley et al., 2015; Soncin et al., 2015, 2018). These include a later specification of TE in the human embryo, and altered/lack of expression of genes, such as EOMES, which are key to mouse TE establishment and expansion (Blakeley et al., 2015; Soncin et al., 2018). As a result of these differences, culture conditions for derivation of mouse trophoblast stem cell cells (TSC), established over 20 years ago (Tanaka et al., 1998), do not give rise to similar cells when applied to human embryos or placental tissues (Kunath et al., 2014).

Recently, distinct culture conditions for derivation and maintenance of human TSC were established, and include EGF, as well as inhibitors of TGFβ and GSK3β (Okae et al., 2018). Variations of this protocol were reported shortly thereafter for the establishment of self-renewing trophoblast organoids (Haider et al., 2018; Turco et al., 2018). Nevertheless, these protocols are only able to establish such cells or organoids from early first trimester (<10 weeks gestational age) human placental tissues and could not be applied to placental tissues at term. This limits the utility of these cells, as, aside from the ethical challenges of using such tissues, the disease potential of these cells is mostly unknown, necessitating development of other model systems from tissues with known pregnancy outcomes.

We previously developed a two-step protocol for differentiation of primed human pluripotent stem cells (hPSC) into terminally-differentiated, functional trophoblast, and demonstrated its use in modeling human trophoblast differentiation in the setting of both normal development and disease (Horii et al., 2016). This protocol uses bone morphogenetic protein-4 (BMP4), which is also known to induce mesoderm in a WNT-dependent manner (Kurek et al., 2015). As such, we recently updated this protocol, applying the WNT inhibitor, IWP2, to the first step, which directs differentiation solely toward the trophoblast lineage (Horii et al., 2019). However, while this protocol produced cells resembling cytotrophoblast (CTB), the proliferative stem cell population in the placenta from which TSC are derived, these cells could not be maintained in a self-renewing state.

Here, we have applied a culture media, recently developed for maintenance of iTSC, reprogrammed from term CTB (Bai et al., 2021), to hPSC-derived CTB, and show that this transitions the cells into bona fide TSC. These cells resemble placenta-derived TSC and can be differentiated into functional syncytiotrophoblast (STB) and extravillous trophoblast (EVT), both *in vitro* and *in vivo*. In addition, we compare these cells to those recently derived from naïve hPSC (Io et al., 2021), and show that they resemble naïve hPSC-derived TSC, both during the transition from pluripotency to TE, and in the final CTB-like state. We conclude that, similar to their naïve counterparts, primed hPSC can be converted to self-renewing TSC following a short induction period with BMP4-containing media.

Results

Generation of TSC-like cells from primed hPSC

We previously developed a two-step protocol for trophoblast differentiation of primed hPSCs (Horii et al., 2019). This protocol involved an initial induction of cells resembling villous cytotrophoblast (CTB), uniformly expressing TP63, using a combination of BMP4 and the WNT inhibitor, IWP2. This led to formation of a uniform group of $EGFR^+$ CTB stem-like cells, which, though not able to self-renew, could be further differentiated, using BMP4 in the presence of feeder-conditioned media, into a mixed set of terminally-differentiated trophoblast, including multinucleated hCG-secreting syncytiotrophoblast (STB) and invasive surface $HLA\text{-}G^+$ extravillous trophoblast (EVT). Nevertheless, this was not only a heterogenous mixture of trophoblast, but also tended to favor STB formation, with only a minority (10-20%) of EVT in the final culture. Here, we applied a new media to CTB stem-like cells at the end of step 1 of our trophoblast differentiation protocol (**Figure 1A**). This media was developed originally by the Kessler lab for reprogramming of term CTB into TSC-like cells (induced TSC/iTSC) (Bai et al., 2021), and is a modification of the Okae media (see Experimental Procedures) used for derivation of TSC from human embryos and early gestation placentae (Okae et al., 2018). After passage in this media at least 5 times, we were able to derive cells morphologically resembling primary TSC (**Figure 1B**) and uniformly expressing cell surface TSC markers, EGFR and ITGA6 (**Figure 1C**). Similar to primary TSC (**Figure S1A**), the hPSC-derived TSC uniformly expressed GATA3 and KRT7 (**Figure 1D**). We successfully derived such cells from both human embryonic stem cell (hESC) lines (WA09/H9 and WA01/H1) and induced pluripotent stem cells (iPSCs) (**Figure S1B**), having been able to keep these cells in culture for over 20 passages.

Characterization of cellular identity of hPSC-derived TSC

We next moved to compare the transcriptome of these cells to primary TSC, which we recently derived from early gestation placental tissues in our own laboratory (Morey et al., 2021),

and have confirmed their identity by direct comparison to the Okae cells (Okae et al., 2018). We isolated RNA from the hPSCs, in both the undifferentiated state and at days 1-4 post trophoblast induction, as well as from hPSC-derived TSC and the two primary TSC lines (1048 and 1049). Principal component analysis (PCA) and K-means clustering separated these samples into three groups, with undifferentiated hPSC and hPSC treated with BMP4-IWP2 for 1 day into one, hPSC treated with BMP4/IWP2 (days 2-4) into a second, and primary and hPSC-derived TSC samples into a third cluster (**Figure 2A**); increasing K did not further separate the samples in a biological meaningful manner (data not shown). The transcriptomes of primary TSC and undifferentiated hPSC were then directly compared (variance = 0.05, two-group analysis $q < 0.05$), leading to the identification of 1618 differentially expressed genes, of which 839 genes were upregulated in TSC and 779 in PSC (**Figure 2B,** and **Supplemental Data S1**). We performed Gene Set Enrichment Analysis (GSEA) and found hPSC-derived TSC were enriched in genes highly expressed in placenta-derived hTSC (padj <0.004, ES=0.44, and NES=2.44) compared to hPSC. We validated expression levels of a handful of TSC-associated markers (TP63, VGLL1, ELF5, ITGA6, and EGFR) by qPCR, and found that the hPSC-derived TSC expressed most of these markers at similar levels to primary hTSC (**Figure 2C**). Similar to primary TSC, hPSC-derived TSC showed uniform expression of TSC markers, including TP63 and CDH1, and lack of pluripotency marker POU5F1/OCT4 (**Figure S2A**). We have previously reported co-expression of CDX2 and TP63 in hPSC following 4 days of BMP4 treatment (Horii et al., 2016), while Okae et al. (2018) have reported low/variable levels of CDX2 expression in primary TSC. We noted that, compared to primary TSC, hPSC-derived TSC showed similar CDX2 levels by qPCR (**Figure 2C**) and a similarly variable nuclear expression of this protein by immunofluorescence (**Figure S2B**).

Primary TSC can only be derived from early first trimester (less than 10 weeks gestational age) cytotrophoblast (CTB) (Okae et al., 2018). We therefore asked how both our primary and hPSC-derived TSC compared to CTB isolated from early (6-8 weeks, CTB_1E) vs. late (10-14 weeks, CTB_1L) first trimester placentae. Transcriptomic analysis showed that both primary and hPSC-derived TSC were distinct from isolated CTB (**Figure S2C**). Unsupervised hierarchical clustering was performed with primary CTB sub-groups combined and independently. The group of samples including both primary and hPSC-derived TSC joined the branch with early first trimester CTB when these cells were included in the analysis, while they joined the branch with undifferentiated and BMP-treated hPSC cells when compared to late first trimester CTB group only (compare left and center dendrograms to the one on the right, in **Figure S2D**).

We next aimed to go beyond the transcriptome, and characterize three other features of early gestation CTB, in our hPSC-derived TSC, namely methylation status of the ELF5 promoter, expression of class I HLA, and expression of the C19 micro RNA (miRNA) cluster. The ELF5 promoter is known to be hypermethylated in hPSCs, but hypomethylated in early gestation CTB (Hemberger et al., 2010) and primary TSC (Okae et al., 2018). Compared to both undifferentiated hPSC and mesenchymal stem cells derived from umbilical cord (Horii et al., 2021), both primary and hPSC-derived TSCs showed significant hypomethylation of this genomic region (**Figure 2D**). In addition to a hypomethylated ELF5 promoter, villous CTB and TSC, which are thought to reside within the CTB layer, are both known to lack expression of class I HLA (HLA-A and HLA-B) (Apps et al., 2009; Io et al., 2021). When we evaluated our cells by flow cytometry, both primary and hPSC-derived TSC expressed class I HLA. Therefore, we re-evaluated our media components and noted that valproic acid (VPA), a histone deacetylase (HDAC) inhibitor, had been previously identified as a compound that promotes class I HLA expression in tumor cells (Armeanu et al.,

2005; Mora-García et al., 2006; Yamanegi et al., 2010; Yang et al., 2020). When we removed this chemical from our media, after only three passages, class I HLA expression significantly decreased in both primary and hPSC-derived TSC (**Figure 2E**), without affecting self-renewal. A third feature of human trophoblast is high expression of the primate-specific, maternally-imprinted C19 micro RNA (miRNA) cluster (Donker et al., 2012; Noguer-Dance et al., 2010). We evaluated the expression of four members of this miRNA cluster, and found that, while hPSC-derived TSC up-regulated one (miR-526b-3p) compared to undifferentiated hPSC, overall, none reached the levels seen in primary TSC and JEG3 choriocarcinoma cells (**Figure S2E**).

It has been argued that, unlike naïve hPSC, primed hPSC give rise to amnion when treated with media containing BMP4 (Guo et al., 2021; Io et al., 2021). To further examine the identity of hPSC-derived TSC, we next evaluated expression of a set of amnion-specific genes in primary TSC, compared to hPSC and their TSC derivatives. We first used an amnion specific gene list, originally published by Roost et al. (Roost et al., 2015): GSEA showed that primary TSC were negatively enriched (NES = -2.18 and padj <0.0005), while hPSC-derived TSC were also not enriched (NES = -1.16 and padj=0.132), for amnion genes. Subsequently, we performed GSEA using an amnion gene list obtained through a more stringent analysis of the Roost et al. (2015), performed by Seetheram et al. (manuscript co-submitted by our collaborators to Stem Cell Reports) (**Figure 2F**). In this GSEA analyses, neither primary nor hPSC-derived TSC were enriched in amnion specific genes (NES = -0.94 with padj= 0.561 and NES = -1.06 with padj= 0.354). Based on these data, as well as the many shared features with primary TSC, we conclude that we have successfully derived TSC-like cells from primed hPSC.

Functional characterization of hPSC-derived TSC

We next moved to characterize the differentiation ability of primed hPSC-derived TSC. When differentiated into STB, they upregulated appropriate markers, including CGA, CGB, GCM1, and PSG4 by qPCR, and secreted hCG into the media, at similar levels as primary TSC-derived STB (**Figure 3A**). Similarly, hPSC-derived TSC could be differentiated into EVT, expressing similar levels of EVT markers, including ASCL2, HLAG, MMP2, HTRA4, ITGA5, and ITGA1, and gaining surface HLA-G expression, similar to primary TSC-derived EVT (**Figure 3B**). Finally, when injected into NOD-SCID mice, both primary and hPSC-derived TSC produced mixed trophoblastic tumors, composed of both hCG^+ and $HLAG^+$ cells (**Figure 3C-D**). Thus, both *in vitro* and *in vivo*, hPSC-derived TSC showed the capacity to differentiate into both terminally-differentiated trophoblast lineages.

Characterizing the path from primed pluripotency to TSC

Our trophoblast induction protocol (Horii et al., 2019) was partially based on a previous study by Kurek et al. (2015), showing that BMP4 induces both trophoblast and mesoderm lineages, where only the latter lineage is WNT-dependent. Thus, the addition of IWP2 should allow exclusive differentiation into trophoblast. We evaluated cells at the end of step 1 (BMP4/IWP2 treatment for 4 days) and noted the gradual flattening of the cells from pluripotency to this stage, and gain of EGFR expression (**Figure 4A**). By qPCR, these cells lost expression of pluripotency factors, and gained expression of markers of trophectoderm (TE), including NR2F2 and CDX2, as well as markers of CTB, including VGLL1 and TP63 (**Figure 4B**); with the exception of DNMT3L, markers of naïve pluripotency were either decreased or only slightly increased (**Figure 4B**). The transition from this state to TSC through several rounds of passage in our modified Okae media was characterized by an initial transition of cells into a mesenchymal morphology, with loss of EGFR, and then a gradual re-epithelialization, with re-gaining of EGFR (**Figure 4C**).

Transcriptomic analysis of this adaptation phase showed unique changes in the gene expression of cells from passage 0 (p0) to p2, before returning back to a signature that more closely resembled primary TSC (**Figure 4D**). Of the 839 genes differentially up-regulated in primary TSC compared to undifferentiated hPSC, 37% (308 genes) were already up-regulated at the end of step I, while 59% (492 genes) were up-regulated in hPSC-derived TSC (**Figure S3A** and **Supplemental Data S2)**. The adaptation did not change the nature of the cells as the most significant tissue-specific signature of all the timepoints was associated with "placenta" (**Figure S3B).** Compared to cells at the end of step 1 (4 days of BMP4/IWP2 treatment), cells at p0 (about 48 hours after being switched to TSC media) demonstrated downregulation of genes associated with apical junction, apoptosis, G2-M checkpoint, and epithelial mesenchymal transition **Supplemental Data S2 and S3**), which correlates with the observed morphology. We performed Click clustering analysis of differentially expressed genes (DEG) across the adaptation phase (**Supplemental Data S4**), which revealed two main patterns of gene expression change (**Figure 4E and Figure S3C**). Cluster #1 included 672 genes that showed an initial progressive downregulation, with lowest expression at p2 of adaptation, followed by subsequent progressive upregulation through p6 (**Figure 4E**). Gene ontology and pathway analysis revealed enrichment in terms associated with cell proliferation, apical junction, and various metabolic processes (**Figure S3D**). Cluster #2 contained 453 genes showing the converse pattern of expression, with a peak at p2 and subsequent downregulation through p6 (**Figure 4E**). GO and pathway analysis showed enrichment in terms associated with epithelial-mesenchymal transition (EMT), which correlate with similarly-noted changes in morphology, as well as apoptosis (**Figure S3D**). Taken together, these data show an adaptive response to hTSC media, involving selection of a subset of cells (through apoptosis and subsequent proliferation), which undergo an EMT process to transition into the TSC state.

Recently, Io et al. (2021) developed a BMP4-based protocol for transitioning naïve hPSCs, first into a TE-like state (after 3 days), characterized by expression of ENPEP, TACSTD2, and NR2F2, and subsequently into a CTB-like state (after 3-15 passages), characterized by SIGLEC6 among other markers (including VGLL1, TP63, and EGFR). We compared our cells to theirs, starting with bulk RNAseq, from primary CTB isolated by both our groups, as well as naïve and primed hPSC and their trophoblast derivatives. Principal component analysis (PCA) showed separation between the naïve and primed hPSC group and primary CTBs (separated along the PC1 axis, 67% variance), with both the naïve and primed hPSC-derived cells located between these two groups on PC1 (**Figure 5A**). Unsupervised hierarchical clustering showed that, while naïve and primed hPSC and their early derivatives (Io's naïve-TE at day 1, and our BMP4/IWP2-treated cells at days 1-2) clustered together, all the later derivatives (Io's naïve-TE at days 2-3, and our BMP4/IWP2-treated cells at days 3-4, as well as both naïve- and primed-hPSC-derived TSC) clustered together with primary CTB (**Figure 5B**). Within the latter group, our BMP4/IWP2-treated cells (at days 3-4) clustered together with Io's naïve-TE (at days 2-3), suggesting the primed cells go through a TE-like phase, while our primed-TSC (at passage 6-8) clustered together with Io's naïve-CTB (at passage 3-15) (**Figure 5B**). Finally, integrating ours and Io's data with two other RNAseq datasets (TSC derived from primed hPSC, by Wei et al. (Wei et al., 2021), and iTSC derived by capturing cellular intermediates during reprogramming of fibroblasts using TSC media, by Liu et al. (Liu et al., 2020)) showed similar results (**Figure S4**). With k=4, the cells clustered as follows: 1) all primary CTB (from first trimester placenta); 2) all TSC, irrespective of the cell of origin (primary, primed or naïve PSC-derived, or directly reprogrammed iTSC); 3) naive PSC at day 0 and induced into TE (days 1-3) as well as BMP4/IWP2-treated primed PSC at days 3-4; and finally 4) all primed PSC as well as BMP4/IWP2-treated primed PSC at days 1-2 (**Figure**

S4). With an increase to k=5, the third cluster (labeled "**C**" in **Figure S4**) broke into two, with the naïve PSC at day 0 and day 1 of TE differentiation in one cluster, and naïve-TE days 2-3 and BMP4-IWP2-treated primed PSC at days 3-4 in the second cluster, again suggesting that the BMP4-IWP2-treated primed hPSC undergo a TE-like phase. A further increase in k did not separate the samples in a biologically meaningful manner (data not shown).

We next evaluated the progression from primed pluripotency to TSC by single cell RNA sequencing (scRNAseq) of H9 hESC, both undifferentiated and treated with BMP4/IWP2 for 12 hours, 24 hours, and 4 days, as well as H9-TSC, using 10X Genomics. A total of 11,259 cells across all timepoints were analyzed by Seurat, which separated the cells into 4 clusters (**Figure 5C**). Cluster 0, despite containing mostly cells at early stages of trophoblast induction with BMP4/IWP2 (12h and 24h), showed a separate transcriptional program from undifferentiated hPSC in cluster 1. Feature plots of pluripotency- and trophoblast-associated genes showed that both clusters 0 and 1 have a strong pluripotency signature (POU5F1 and NANOG), with a subset of cluster 0 cells initiating the TE program, as noted by GATA3 expression, as early as 12 hours from induction. Cluster 3 cells (those treated with BMP4/IWP2 for 4 days) had completely lost NANOG expression, but had begun to express TE-associated genes, including KRT19, ENPEP, TACSTD2, and NR2F2, similar to Io's naïve PSC-derived TE (Io et al., 2021) (**Figure 5C**). As TSCs, cells gained expression of CTB-associated genes, including EGFR, VGLL1, and SIGLEC6, similar to Io's naïve PSC-derived CTB (Io et al., 2021) (**Figure 5C**). Naïve pluripotency markers were expressed at low levels in rare undifferentiated primed hPSC but (with the exception of DNMT3L) they were absent in BMP4/IWP2-treated hPSC (**Figure 5C**). When we evaluated our scRNAseq cell clusters using epiblast (EPI) and TE gene signatures obtained from day 6-10 extended culture human embryos (Zhou et al., 2019) (**Supplemental Data S5**), clusters 0 and 1

showed enrichment in EPI-specific genes, while clusters 2 and 3 showed enrichment in TE-specific genes (**Figure 5D**). Finally, when the transcriptomic signatures of hPSC at day 4 of BMP4/IWP2 treatment as well as both primary and hPSC-derived TSC were compared to undifferentiated hPSC and analyzed by the PlacentaCellEnrich tool (Jain and Tuteja, 2021), all 3 groups showed highest enrichment of genes from trophoblast cells in the placenta, with similar enrichment for syncytiotrophoblast (STB)-, extravillous trophoblast (EVT)-, and cytotrophoblast (CTB)-associated genes (**Figure 5E**). These data suggest that primed hPSC have the potential to give rise to TSC, following induction into a TE-like phase with 4 days of treatment with BMP4/IWP2, providing a simple protocol for obtaining TSC from a vast array of available embryonic and induced pluripotent stem cells.

Discussion

The modeling of human trophoblast differentiation has proven difficult for multiple reasons, including significant divergence of factors regulating early embryonic development (Blakeley et al., 2015), as well as the establishment and maintenance of human trophoblast stem cells (Okae et al., 2018). We previously showed that BMP4-mediated trophoblast differentiation of hPSC requires TP63 (specifically, the N-terminally truncated isoform, ΔN-p63α) (Li et al., 2013), a transcription factor that is widely expressed in stem cells of stratified epithelia, including villous CTB of the human placenta (Lee et al., 2007) and helps maintain these cells in their undifferentiated state (Haider et al., 2016; Li et al., 2014). Another transcription factor uniquely expressed in human TSC is VGLL1, a potential co-factor for TEAD4 in this setting (Okae et al., 2018; Saha et al., 2020; Soncin et al., 2018). This contrasts with mouse TSC, where CDX2 and EOMES play key roles in establishment and/or maintenance (Russ et al., 2000; Strumpf et al.,

2005). CDX2 is expressed in human TE and a subset of first trimester villous CTB (Blakeley et al., 2015; Horii et al., 2016; Soncin et al., 2018); however, its expression is minimal (though variable) in established human TSC lines (Okae et al., 2018), and thus it is unclear whether it in fact plays a role in human TSC maintenance. EOMES is completely absent from both human TE and villous CTB at any gestational age (Blakeley et al., 2015; Soncin et al., 2018). Another transcription factor required for mouse TSC maintenance is Elf5 (Donnison et al., 2005). In human, ELF5 is expressed in both villous CTB as well as some cells of the trophoblast column (immature extravillous trophoblast) (Hemberger et al., 2010; Soncin et al., 2018), though its exact role in human TSC establishment and maintenance remains unknown. Further, while it is unclear how closely its expression in human trophoblast is tied to its promoter methylation, that its promoter is hypomethylated in early gestation trophoblast (particularly in comparison to undifferentiated hPSC) has been fully established (Hemberger et al., 2010; Okae et al., 2018). Our hPSC-derived TSC express all three of these transcription factors (TP63, VGLL1, and ELF5) at similar-to-higher levels than primary placenta-derived TSC, have a similarly-variable expression of CDX2, and show proper hypomethylation of ELF5 promoter, compared to their pluripotent cells-of-origin. One difference, however, remains with primary hTSC: that is, insufficient upregulation of C19MC miRNA's. It is well-known that these miRNA's are maternally imprinted, their expression tightly regulated by DNA methylation (Noguer-Dance et al., 2010); thus it is likely that additional manipulation of culture media is required to further enhance their expression in hPSC-derived TSC. While the high expression of this class of miRNA's is a defining feature of human trophoblast (Donker et al., 2012), their exact role in primary hTSC maintenance and differentiation remain to be explored; therefore, at least for now, the significance of insufficient induction of these miRNA's in hPSC-derived TSC remains unknown.

Despite this difference in C19MC miRNA expression, our hPSC-derived TSC fully recapitulate primary TSC function. They are able to differentiate into both hCG-producing syncytiotrophoblast (STB) and surface HLAG-expressing extravillous trophoblast (EVT). This differentiation potential was recapitulated *in vivo*, by their ability to form trophoblastic tumors in immunocompromised mice, with the typical necrotic center and expression of STB- and EVT-associated markers. Such features of the hPSC-derived TSC functionally define their true identity as trophoblast, and exclude other identities, including amnion. In addition to transcriptomic differences, as described both in our current manuscript and, in significantly more detail by Seetharam et al. in the same issue of this journal, normal amniotic epithelium is a simple cuboidal epithelium, lacking expression of TP63 (Li et al., 2013). Rare reports of amnion expressing HLA-G do not cite specific antibodies used, and in fact, report co-expression of class I HLA molecules in these cells (Strom and Gramignoli, 2016); similarly, the single report of hCG expression in early amnion within the developing human embryo (Xiang et al., 2020) show staining in a simple, non-stratified epithelium, rather than the secretory ability of a stem cell, following forskolin-induced syncytialization, as occurs in primary TSC. When morphologic features and marker expression are considered together, hPSC-derived TSC most closely resemble primary, placenta-derived TSC, and are clearly distinct from amniotic epithelium.

Perhaps the most difficult-to-explain aspect of the trophoblast differentiation ability of primed hPSC is the developmental trajectory of these cells. The initial segregation of the TE lineage follows the transition from totipotency (2-cell/2C state) to naïve pluripotency, which is the defining feature of pre-implantation inner cell mass/ICM or epiblast (Baker and Pera, 2018; Dong et al., 2019; Rossant and Tam, 2017). It has been suggested that, at least in mouse, this process of lineage segregation into TE and ICM is in fact epigenetically irreversible, precluding mouse ESC

transdifferentiated into TSC-like cells (e.g. by overexpression of Cdx2) to significantly contribute to the trophoblast compartment (Cambuli et al., 2014). Primed hPSC are considered equivalent to post-implantation epiblast, a stage of development far beyond TE development, and thus, by definition, should not have the potential to generate TE (De Los Angeles, 2019). In fact, in mouse, both naïve and primed ESC exclusively give rise to epiblast-derived cells when injected into proper stage embryos (Huang et al., 2012; Ying et al., 2008). However, unlike naïve mouse ESC, naïve human ESC have recently been shown by multiple groups to readily give rise to trophoblast (Cinkornpumin et al., 2020; Dong et al., 2020; Guo et al., 2021; Io et al., 2021), suggesting greater plasticity of human ESC. In addition, it has been shown that media containing BMP4 induces chromatin remodeling in primed mouse ESC (Kime et al., 2016; Yu et al., 2020), inducing some cells toward a naïve, and even 2C-like, fate, while producing TE-like features in other cells (Kime et al., 2019; Tomoda et al., 2021). Our own analysis of primed hPSC treated with BMP4-containing media points to a direct conversion of these cells to a TE-like fate, following 4 days of treatment with BMP4 and IWP2, with induction of only one naïve pluripotency marker noted. Comparison to Io et al.'s (2021) naïve hPSC-derived cells also showed that primed hPSC treated with BMP4/IWP2 clustered with naïve TE, not naïve hPSC, thus suggesting differentiation into TSC through a TE intermediate. In addition, comparison of our single cell RNAseq data to that of extended culture human embryos (Zhou et al., 2019) also showed that BMP4/IWP2-treated primed hPSC have a gene signature resembling TE, not epiblast. Finally, recent reports have shown that direct reprogramming of human fibroblasts to a TSC-like fate can occur when Yamanaka pluripotency factors are applied to the cells, and the media switched from one used for culture of hPSC (E7) to Okae's TSC media during reprogramming (Castel et al., 2020). Analysis of the reprogramming process suggests that iTSC can be captured from a TE-like subpopulation, without

initial formation of naïve hPSC intermediates (Liu et al., 2020), suggesting perhaps greater plasticity, and fewer epigenetic barriers, between early human stem cell lineages.

Our protocol offers a relatively simple way to convert the many existing hPSC lines, including induced pluripotent stem cells representing many diseases, into TSC-like cells, thus allowing researchers broad access to platforms for human placental research, even where this research may be limited by lack of access to first trimester placental tissues. Another group has recently published a similar study, showing a role for BMP4 in accelerating transition of primed hPSC into TSC (Wei et al., 2021). Nevertheless, much work, and many questions, remain, including how primed hPSC-derived TSC compare to similar cells derived from naïve hPSC, not just in their DNA methylation patterns, but in other aspects of their epigenome (including their chromatin and miRNA landscape) as well as their ability to recapitulate trophoblast-based disorders of the placenta. In addition, the different pluripotent states of human ESC, as well as TE and TSC, deserve further study in context of the human embryo, including the extent of their lineage segregation as well as the role of BMP4 in potentially enhancing inter-conversion.

Experimental Procedures

Conversion of hPSC-derived TE to TSC-like cells

Following the first-step of trophoblast differentiation from the previously published protocol (Horii et al., 2019) (see also supplemental experimental procedures), hPSC-derived TE-like cells were dissociated using TrypLE Express (ThermoFisher) and pelleted by centrifugation at 1000 rpm for 5min. hPSC-derived TE-like cells were resuspended in TSC media and plated with a 1:1 split ratio onto collagen IV (MilliporeSigma, 5µg/mL) coated plates. We used TSC media that was established in the laboratory of Dr. John Kessler for optimal growth and passage of primary term

CTB reprogrammed into self-renewing TSC-like cells (Bai et al., 2021), which is composed of: Advanced DMEM/F12 (ThermoFisher), 1x N2 (ThermoFisher), 1x B27 (ThermoFisher), 1x Glutmax (ThermoFisher), 150μM 1-thioglycerol (MilliporeSigma), 0.05% BSA (Gemini), 1% Knockout serum replacement (KSR, ThermoFisher), 2μM CHIR99021 (MilliporeSigma), 0.5μM A83-01 (Tocris), 1μM SB431542 (MilliporeSigma), 5μM Y27632 (Selleck Chemicals), 130μg/mL Valproic Acid sodium salt (MilliporeSigma), 100ng/mL recombinant human FGF2 (BioPioneer), 50ng/mL recombinant human EGF (R&D Systems), 50ng/mL recombinant human HGF (Stem Cell Technologies), and 20ng/mL Noggin (R&D System). Media was replenished every day. Cells were passaged using TrypLE when confluent (approximately every other day) with a split ratio of 1:2 onto collagen IV coated plates. Conversion into TSC was deemed complete after at least 5 passages with surface EGFR expression of over 90%, and HLA-G expression of 20% or less, by flow cytometry.

Statistical analysis

All experiments were performed in triplicate. Bar chart data display mean fold change and standard deviation of the mean. Statistical analysis was done using GraphPad Prism 9. Student's t-test was performed to determine significance of differences between groups, and the level of significance is represented with * as indicated in the figures.

Data and Code Availability

RNAseq data have been deposited to the Gene Expression Omnibus database under the accession number GSE182791. The 10 samples of CTB from late first trimester (CTB_1L) were previously deposited in GEO under GSE173323 (Morey et al., 2021).

Acknowledgements

This work was supported by funds from the National Institutes of Health (NIH)/National Institute of Child Health and Human Development (NICHD) (R01HD-089537 to MMP; K99-R00-HD091452 to MH; and R01-HD096260 to FS), and the UC San Diego Stem Cell Program. RM and VCC were supported by a grant from the National Institutes of Health, USA (NIH grant T32GM8806). JD was supported by a grant from the American Society for Reproductive Medicine. MGJ was supported by the Bridges to Stem Cell Research Internship Program Grant from the CIRM (EDUC2-08388). We thank Elsa Molina, PhD, Director of the UC San Diego Stem Cell Genomics & Microscopy Core for her expert assistance with the single-cell RNAseq experiments. The manuscript also includes data generated at the UC San Diego IGM Genomics Center utilizing an Illumina NovaSeq 6000 that was purchased with funding from a National Institutes of Health SIG grant (#S10 OD026929). The work was also partially supported by the National Institutes of Health, Grant 2UL1TR001442-06 of CTSA; the content is solely the responsibility of the authors and does not necessarily represent the official views of the NIH. Finally, this publication used the Extreme Science and Engineering Discovery Environment (XSEDE) Comet for computational analysis, which is supported by National Science Foundation grant number ACI-1548562 (allocation ID: TG-MCB140074).

Author contributions

FS, RM, TB, DFR, VCC, SK, RK, MGJ, OF, DP, and MH performed the experiments. MM consented patients and collected samples for this study. FS, RM, DFR, JD and KF performed the data analysis. FS, MH, and MMP designed and supervised the study. FS, RM, VCC, and MMP wrote the manuscript.

Declaration of Interests

The authors declare no competing interests.

References

Apps, R., Murphy, S.P., Fernando, R., Gardner, L., Ahad, T., and Moffett, A. (2009). Human leucocyte antigen (HLA) expression of primary trophoblast cells and placental cell lines, determined using single antigen beads to characterize allotype specificities of anti-HLA antibodies. Immunology *127*, 26–39.

Armeanu, S., Bitzer, M., Lauer, U.M., Venturelli, S., Pathil, A., Krusch, M., Kaiser, S., Jobst, J., Smirnow, I., Wagner, A., et al. (2005). Natural Killer Cell–Mediated Lysis of Hepatoma Cells via Specific Induction of NKG2D Ligands by the Histone Deacetylase Inhibitor Sodium Valproate. Cancer Res. *65*, 6321–6329.

Bai, T., Peng, C.Y., Aneas, I., Sakabe, N., Requena, D.F., Billstrand, C., Nobrega, M., Ober, C., Parast, M., and Kessler, J.A. (2021). Establishment of human induced trophoblast stem-like cells from term villous cytotrophoblasts. Stem Cell Res. *56*, 102507.

Baker, C.L., and Pera, M.F. (2018). Capturing Totipotent Stem Cells. Cell Stem Cell *22*, 25–34.

Blakeley, P., Fogarty, N.M.E., Valle, I., Wamaitha, S.E., Hu, T.X., Elder, K., Snell, P., Christie, L., Robson, P., Niakan, K.K., et al. (2015). Defining the three cell lineages of the human blastocyst by single-cell RNA-seq (Development, (2015) 142, 3151-3165). Dev. *142*, 3613.

Burton, G.J., and Jauniaux, E. (2015). What is the placenta? Am. J. Obstet. Gynecol. *213*, S6.e1-S6.e4.

Cambuli, F., Murray, A., Dean, W., Dudzinska, D., Krueger, F., Andrews, S., Senner, C.E.,

Cook, S.J., and Hemberger, M. (2014). Epigenetic memory of the first cell fate decision prevents complete ES cell reprogramming into trophoblast. Nat. Commun. *5*.

Castel, G., Meistermann, D., Bretin, B., Firmin, J., Blin, J., Loubersac, S., Bruneau, A., Chevolleau, S., Kilens, S., Chariau, C., et al. (2020). Induction of Human Trophoblast Stem Cells from Somatic Cells and Pluripotent Stem Cells. Cell Rep. *33*.

Cinkornpumin, J.K., Kwon, S.Y., Guo, Y., Hossain, I., Sirois, J., Russett, C.S., Tseng, H.W., Okae, H., Arima, T., Duchaine, T.F., et al. (2020). Naive Human Embryonic Stem Cells Can Give Rise to Cells with a Trophoblast-like Transcriptome and Methylome. Stem Cell Reports *15*, 198–213.

Dong, C., Fischer, L.A., and Theunissen, T.W. (2019). Recent insights into the naïve state of human pluripotency and its applications. Exp. Cell Res. *385*.

Dong, C., Beltcheva, M., Gontarz, P., Zhang, B., Popli, P., Fischer, L.A., Khan, S.A., Park, K.M., Yoon, E.J., Xing, X., et al. (2020). Derivation of trophoblast stem cells from naïve human pluripotent stem cells. Elife *9*, 1–26.

Donker, R.B., Mouillet, J.F., Chu, T., Hubel, C.A., Stolz, D.B., Morelli, A.E., and Sadovsky, Y. (2012). The expression profile of C19MC microRNAs in primary human trophoblast cells and exosomes. Mol. Hum. Reprod. *18*, 417–424.

Donnison, M., Beaton, A., Davey, H.W., Broadhurst, R., L'Huillier, P., and Pfeffer, P.L. (2005). Loss of the extraembryonic ectoderm in Elf5 mutants leads to defects in embryonic patterning. Development *132*, 2299–2308.

Guo, G., Stirparo, G.G., Strawbridge, S.E., Spindlow, D., Yang, J., Clarke, J., Dattani, A., Yanagida, A., Li, M.A., Myers, S., et al. (2021). Human naive epiblast cells possess unrestricted lineage potential. Cell Stem Cell *28*, 1040-1056.e6.

Haider, S., Meinhardt, G., Saleh, L., Fiala, C., Pollheimer, J., and Knöfler, M. (2016). Notch1 controls development of the extravillous trophoblast lineage in the human placenta. Proc. Natl. Acad. Sci. U. S. A. *113*, E7710–E7719.

Haider, S., Meinhardt, G., Saleh, L., Kunihs, V., Gamperl, M., Kaindl, U., Ellinger, A., Burkard, T.R., Fiala, C., Pollheimer, J., et al. (2018). Self-Renewing Trophoblast Organoids Recapitulate the Developmental Program of the Early Human Placenta. Stem Cell Reports *11*, 537–551.

Hemberger, M., Udayashankar, R., Tesar, P., Moore, H., and Burton, G.J. (2010). ELF5-enforced transcriptional networks define an epigenetically regulated trophoblast stem cell compartment in the human placenta. Hum. Mol. Genet. *19*, 2456–2467.

Horii, M., Li, Y., Wakeland, A.K., Pizzo, D.P., Nelson, K.K., Sabatini, K., Laurent, L.C., Liu, Y., and Parast, M.M. (2016). Human pluripotent stem cells as a model of trophoblast differentiation in both normal development and disease. Proc. Natl. Acad. Sci. U. S. A. *113*, E3882–E3891.

Horii, M., Bui, T., Touma, O., Cho, H.Y., and Parast, M.M. (2019). An Improved Two-Step Protocol for Trophoblast Differentiation of Human Pluripotent Stem Cells. Curr. Protoc. Stem Cell Biol. *50*, 1–21.

Horii, M., Morey, R., Bui, T., Touma, O., Nelson, K.K., Cho, H.Y., Rishik, H., Laurent, L.C., and Parast, M.M. (2021). Modeling preeclampsia using human induced pluripotent stem cells. Sci. Rep. *11*.

Huang, Y., Osorno, R., Tsakiridis, A., and Wilson, V. (2012). In Vivo Differentiation Potential of Epiblast Stem Cells Revealed by Chimeric Embryo Formation. Cell Rep. *2*, 1571–1578.

Io, S., Kabata, M., Iemura, Y., Semi, K., Morone, N., Minagawa, A., Wang, B., Okamoto, I., Nakamura, T., Kojima, Y., et al. (2021). Capturing human trophoblast development with naive

pluripotent stem cells in vitro. Cell Stem Cell *28*, 1023-1039.e13.

Jain, A., and Tuteja, G. (2021). PlacentaCellEnrich: A tool to characterize gene sets using placenta cell-specific gene enrichment analysis. Placenta *103*, 164–171.

Kime, C., Sakaki-Yumoto, M., Goodrich, L., Hayashi, Y., Sami, S., Derynck, R., Asahi, M., Panning, B., Yamanaka, S., and Tomoda, K. (2016). Autotaxin-mediated lipid signaling intersects with LIF and BMP signaling to promote the naive pluripotency transcription factor program. Proc. Natl. Acad. Sci. U. S. A. *113*, 12478–12483.

Kime, C., Kiyonari, H., Ohtsuka, S., Kohbayashi, E., Asahi, M., Yamanaka, S., Takahashi, M., and Tomoda, K. (2019). Induced 2C Expression and Implantation-Competent Blastocyst-like Cysts from Primed Pluripotent Stem Cells. Stem Cell Reports *13*, 485–498.

Kunath, T., Yamanaka, Y., Detmar, J., MacPhee, D., Caniggia, I., Rossant, J., and Jurisicova, A. (2014). Developmental differences in the expression of FGF receptors between human and mouse embryos. Placenta *35*, 1079–1088.

Kurek, D., Neagu, A., Tastemel, M., Tüysüz, N., Lehmann, J., Van De Werken, H.J.G., Philipsen, S., Van Der Linden, R., Maas, A., Van Ijcken, W.F.J., et al. (2015). Endogenous WNT signals mediate BMP-induced and spontaneous differentiation of epiblast stem cells and human embryonic stem cells. Stem Cell Reports *4*, 114–128.

Lee, Y., Kim, K.R., McKeon, F., Yang, A., Boyd, T.K., Crum, C.P., and Parast, M.M. (2007). A unifying concept of trophoblastic differentiation and malignancy defined by biomarker expression. Hum. Pathol. *38*, 1003–1013.

Li, Y., Moretto-Zita, M., Soncin, F., Wakeland, A., Wolfe, L., Leon-Garcia, S., Pandian, R., Pizzo, D., Cui, L.L., Nazor, K., et al. (2013). BMP4-directed trophoblast differentiation of human embryonic stem cells is mediated through a ΔNp63+ cytotrophoblast stem cell state. Dev.

140, 3965–3976.

Li, Y., Moretto-Zita, M., Leon-Garcia, S., and Parast, M.M. (2014). P63 inhibits extravillous trophoblast migration and maintains cells in a cytotrophoblast stem cell-like state. Am. J. Pathol. *184*, 3332–3343.

Liu, X., Ouyang, J.F., Rossello, F.J., Tan, J.P., Davidson, K.C., Valdes, D.S., Schröder, J., Sun, Y.B.Y., Chen, J., Knaupp, A.S., et al. (2020). Reprogramming roadmap reveals route to human induced trophoblast stem cells. Nature *586*, 101–107.

De Los Angeles, A. (2019). Frontiers of Pluripotency. Methods Mol. Biol. *2005*, 3–27.

Mora-García, M. de L., Duenas-González, A., Hernández-Montes, J., De la Cruz-Hernández, E., Pérez-Cárdenas, E., Weiss-Steider, B., Santiago-Osorio, E., Ortíz-Navarrete, V.F., Rosales, V.H., Cantú, D., et al. (2006). Up-regulation of HLA class-I antigen expression and antigen-specific CTL response in cervical cancer cells by the demethylating agent hydralazine and the histone deacetylase inhibitor valproic acid. J. Transl. Med. *4*.

Morey, R., Farah, O., Kallol, S., Requena, D.F., Meads, M., Moretto-Zita, M., Soncin, F., Laurent, L.C., and Parast, M.M. (2021). Transcriptomic Drivers of Differentiation, Maturation, and Polyploidy in Human Extravillous Trophoblast. Front. Cell Dev. Biol. *9*.

Niakan, K.K., Han, J., Pedersen, R.A., Simon, C., and Pera, R.A.R. (2012). Human pre-implantation embryo development. Development *139*, 829–841.

Noguer-Dance, M., Abu-Amero, S., Al-Khtib, M., Lefèvre, A., Coullin, P., Moore, G.E., and Cavaillé, J. (2010). The primate-specific microRNA gene cluster (C19MC) is imprinted in the placenta. Hum. Mol. Genet. *19*, 3566–3582.

Okae, H., Toh, H., Sato, T., Hiura, H., Takahashi, S., Shirane, K., Kabayama, Y., Suyama, M., Sasaki, H., and Arima, T. (2018). Derivation of Human Trophoblast Stem Cells. Cell Stem Cell

22, 50-63.e6.

Roost, M.S., Van Iperen, L., Ariyurek, Y., Buermans, H.P., Arindrarto, W., Devalla, H.D., Passier, R., Mummery, C.L., Carlotti, F., De Koning, E.J.P., et al. (2015). KeyGenes, a Tool to Probe Tissue Differentiation Using a Human Fetal Transcriptional Atlas. Stem Cell Reports *4*, 1112–1124.

Rossant, J., and Tam, P.P.L. (2017). New Insights into Early Human Development: Lessons for Stem Cell Derivation and Differentiation. Cell Stem Cell *20*, 18–28.

Russ, A.P., Wattler, S., Colledge, W.H., Aparicio, S.A.J.R., Carlton, M.B.L., Pearce, J.J., Barton, S.C., Azim Surani, M., Ryan, K., Nehls, M.C., et al. (2000). Eomesodermin is required for mouse trophoblast development and mesoderm formation. Nature *404*, 95–99.

Saha, B., Ganguly, A., Home, P., Bhattacharya, B., Ray, S., Ghosh, A., Karim Rumi, M.A., Marsh, C., French, V.A., Gunewardena, S., et al. (2020). TEAD4 ensures postimplantation development by promoting trophoblast self-renewal: An implication in early human pregnancy loss. Proc. Natl. Acad. Sci. U. S. A. *117*, 17864–17875.

Soncin, F., Natale, D., and Parast, M.M. (2015). Signaling pathways in mouse and human trophoblast differentiation: A comparative review. Cell. Mol. Life Sci. *72*.

Soncin, F., Khater, M., To, C., Pizzo, D., Farah, O., Wakeland, A., Rajan, K.A.N.K.A.N., Nelson, K.K.K.K., Chang, C.-W.C.W., Moretto-Zita, M., et al. (2018). Comparative analysis of mouse and human placentae across gestation reveals species-specific regulators of placental development. Dev. *145*.

Strom, S.C., and Gramignoli, R. (2016). Human amnion epithelial cells expressing HLA-G as novel cell-based treatment for liver disease. Hum. Immunol. *77*, 734–739.

Strumpf, D., Mao, C.A., Yamanaka, Y., Ralston, A., Chawengsaksophak, K., Beck, F., and

Rossant, J. (2005). Cdx2 is required for correct cell fate specification and differentiation of trophectoderm in the mouse blastocyst. Development *132*, 2093–2102.

Tanaka, S., Kunath, T., Hadjantonakis, A.K., Nagy, A., and Rossant, J. (1998). Promotion to trophoblast stem cell proliferation by FGF4. Science (80-.). *282*, 2072–2075.

Tomoda, K., Hu, H., Sahara, Y., Sanyal, H., Takasato, M., and Kime, C. (2021). Reprogramming epiblast stem cells into pre-implantation blastocyst cell-like cells. Stem Cell Reports *16*, 1197–1209.

Turco, M.Y., Gardner, L., Kay, R.G., Hamilton, R.S., Prater, M., Hollinshead, M.S., McWhinnie, A., Esposito, L., Fernando, R., Skelton, H., et al. (2018). Trophoblast organoids as a model for maternal–fetal interactions during human placentation. Nature *564*, 263–281.

Wei, Y., Wang, T., Ma, L., Zhang, Y., Zhao, Y., Lye, K., Xiao, L., Chen, C., Wang, Z., Ma, Y., et al. (2021). Efficient derivation of human trophoblast stem cells from primed pluripotent stem cells. Sci. Adv. *7*.

Xiang, L., Yin, Y., Zheng, Y., Ma, Y., Li, Y., Zhao, Z., Guo, J., Ai, Z., Niu, Y., Duan, K., et al. (2020). A developmental landscape of 3D-cultured human pre-gastrulation embryos. Nature *577*, 537–542.

Yamanegi, K., Yamane, J., Kobayashi, K., Kato-Kogoe, N., Ohyama, H., Nakasho, K., Yamada, N., Hata, M., Nishioka, T., Fukunaga, S., et al. (2010). Sodium valproate, a histone deacetylase inhibitor, augments the expression of cell-surface NKG2D ligands, MICA/B, without increasing their soluble forms to enhance susceptibility of human osteosarcoma cells to NK cell-mediated cytotoxicity. Oncol. Rep. *24*, 1621–1627.

Yang, W., Li, Y., Gao, R., Xiu, Z., and Sun, T. (2020). MHC class I dysfunction of glioma stem cells escapes from CTL-mediated immune response via activation of Wnt/β-catenin signaling

pathway. Oncogene *39*, 1098–1111.

Ying, Q.L., Wray, J., Nichols, J., Batlle-Morera, L., Doble, B., Woodgett, J., Cohen, P., Smith, A., Johansson, B.M., Wiles, M. V, et al. (2008). The ground state of embryonic stem cell self-renewal. Nature *448*, 519–523.

Yu, S., Zhou, C., Cao, S., He, J., Cai, B., Wu, K., Qin, Y., Huang, X., Xiao, L., Ye, J., et al. (2020). BMP4 resets mouse epiblast stem cells to naive pluripotency through ZBTB7A/B-mediated chromatin remodelling. Nat. Cell Biol. *22*, 651–662.

Zhou, F., Wang, R., Yuan, P., Ren, Y., Mao, Y., Li, R., Lian, Y., Li, J., Wen, L., Yan, L., et al. (2019). Reconstituting the transcriptome and DNA methylome landscapes of human implantation. Nature *572*, 660–664.

Figure Titles and Legends

Figure 1. Protocol for conversion of primed hPSC into TSC. **A)** Protocol schematic. **B)** Morphology of H9 hESC line as undifferentiated (day 0), following 4 days of BMP4/IWP2 treatment (day 4), and after 5 passages in our modified Okae media for TSC (H9-TSC). **C)** Flow cytometric analysis of H9-derived TSC for EGFR and ITGA6. **D)** Immunofluorescence staining of H9-TSC for GATA3 and KRT7. Bar=124.5 μm. Data in B, C, and D are representative of n = 5 independent experiments. See also **Figure S1**.

Figure 2. Characterization of hPSC-derived TSC. **A)** Principal Component Analysis of hPSC (undifferentiated/day 0), H9 hESC treated with BMP4/IWP2 for 1-4 days, hPSC-derived TSC after 6-8 passages in the modified Okae TSC media (TSC), and primary (placenta-derived) TSC (lines 1048 and 1049). Each dot on the PCA represents a sample from an independent experiment (n = 2

for H1 and iPSC, day 0 and TSC; n = 3 for all other samples). Sample clusters from k-means clustering, marked by circles, show that hPSC-derived TSC cluster together with primary (placenta-derived) hTSC. **B)** Heatmaps of undifferentiated hPSC, and primary and hPSC-derived TSC, showing genes that are either upregulated (839 genes) or downregulated (779 genes) in primary TSC in comparison to undifferentiated hPSC. GSEA showed that hPSC-derived TSC were enriched in primary TSC-associated genes (NES 2.44, padj<0.004), but not in (undifferentiated) hPSC-associated genes. A few TSC-associated genes are noted in the heatmap. **C)** qPCR of the indicated CTB markers in undifferentiated primary TSC (1049) compared to hPSC (H9)-TSC. Data were normalized to L19 and shown as fold change over undifferentiated 1049 (D0=day 0), and represent mean +/- SD for n = 3 independent experiments. *p < 0.05; **p < 0.01 by student's t-test. **D)** DNA methylation surrounding the ELF5 promoter in undifferentiated (U) H9 ESC, TSC derived from both H9 and a human dermal fibroblast (HDF)-derived iPSC, an umbilical cord derived mesenchymal stem cell line (1754), and a primary (placenta-derived) TSC line (1049). Each line represents a distinct sequenced clone (n = 3 to 9). **E)** Flow cytometric analysis of primary (1049) and hPSC (H9)-derived TSC for HLA-A2 and HLA-Bw6 with (grey) and without (purple) valproic acid (VPA) in the culture media. Data are representative of 2 independent experiments. **F)** Heatmap of amnion-specific markers (based on a more stringent analysis by Seetheram et al., in this issue of Stem Cell Reports, of the Roost et al., 2015 dataset) in undifferentiated hPSC, primary (1048 and 1049 TSC) and hPSC-derived TSC, as well as amnion (AM). GSEA showed that neither primary nor hPSC-derived TSC were enriched in amnion-specific genes (NES = -0.94 with padj= 0.561 and NES = -1.06 with padj= 0.354, respectively). See also **Figure S2**.

Figure 3. *In vitro* and *in vivo* differentiation potential of hPSC-derived TSC. **A)** Morphology, lineage-specific gene expression, and hCG secretion of primary (1049) and hPSC (H9)-derived TSC differentiated into syncytiotrophoblast (STB). qPCR data were normalized to L19 and shown as fold change over undifferentiated (day 0/D0) 1049 TSC. hCG secretion was normalized to ng of DNA. Both qPCR and ELISA data represent mean +/- SD for n = 3 independent experiments. *$p < 0.05$; **$p < 0.01$ by student's t-test. **B)** Morphology, lineage-specific gene expression, and flow cytometric analysis for surface HLA-G expression of primary (1049) and hPSC (H9)-derived TSC differentiated into extravillous trophoblast (EVT). qPCR data were normalized to L19 and shown as fold change over undifferentiated (day 0/D0) 1049 TSC, and represent mean +/- SD for n = 3 independent experiments. *$p < 0.05$; **$p < 0.01$; ***$p < 0.001$ by student's t-test. Flow cytometric data are representative of 3 independent experiments. **C and D)** Tumors generated 10 days following injection of primary (1049) and hPSC (H9)-derived TSC into NOD-SCID mice (representative of n = 2 independent experiments). **C)** H&E staining shows the tumor cells invading through muscle (1049-TSC tumor) or forming a tumor with a necrotic center (H9-TSC), both characteristic of human trophoblastic tumors. Scale bars = 250μm for low-power images (left) or 50μm for high-power images (right). **D)** Immunohistochemical staining of the same tumors using antibodies against EGFR, hCG, and HLAG shows positively-stained cells (brown) in the TSC-derived lesions. Scale bars = 50μm.

Figure 4. Transition from primed pluripotency to TSC involves a trophectoderm-like intermediate. **A)** Morphology of H9-ESC at days 0, 2, and 4 following treatment with BMP4/IWP2. At the end of 4 days, over 94% of the cells express EGFR by flow cytometric analysis. Data are representative of n = 5 independent experiments. **B)** qPCR of H9-ESC at days 0, 2, and 4 following BMP4/IWP2

treatment, for markers of pluripotency (NANOG and POU5F1), naïve pluripotency (DNMT3L, KLF17, DPPA3, and DPPA5), trophectoderm (ENPEP, TACSTD2, NR2F2, and CDX2), and cytotrophoblast (CTB) (TP63, VGLL1, GATA2, GATA3, TFAP2C). Data were normalized to L19 and shown as fold change over undifferentiated H9-ESC (D0=day 0). *$p < 0.05$; **$p < 0.01$; ***$p < 0.001$; ****$p < 0.0001$ by student's t-test. **C)** Morphology and EGFR expression of BMP4/IWP2-treated H9-ESC, passaged in modified Okae TSC media. During this time, the cells initially lose EGFR expression and slowly re-gain it after at least 5 passages. Data are representative of n = 3 independent experiments. **D)** Principal component analysis of cells transitioning from primed pluripotency (hPSC) through BMP4/IWP2 induction, then undergoing adaptation through 6 passages (p0-p6) in modified Okae TSC media. Arrow points to passage in which the hPSC-derived cells are farthest away from primary TSC. Each dot on the PCA represents a sample from an independent experiment (n = 2 for H1 and iPSC, day 0 and TSC; n = 3 for all H9 samples). **E)** Median expression of genes in clusters 1 and 2 from Click-clustering analysis **Figure S3C-D**) of H9-ESC at day 4 of BMP4/IWP2 treatment and across TSC media adaptation (10 sample groups indicated by red box in **D**). See also **Figure S3**.

Figure 5. Comparison of trophectoderm and TSC derived from naïve and primed hPSC. **A)** Principal component analysis of our cells, combined with those published by Io et al. [15], including, from left to right: 1) undifferentiated naïve and primed hPSC (day 0) and their early trophoblast derivatives (days 1-2 in our BMP4/IWP2 treatment, and day 1 of Io et al.'s induction); 2) naïve and primed hPSC induced into a trophectoderm/TE-like fate (days 3-4 in our BMP4/IWP2 treatment, and days 2-3 of Io et al.'s induction); 3) primary (placenta-derived) TSC (1048 and 1049 lines), our primed hPSC-derived TSC (H9-TSC at passage 6, H1-TSC at passage 7, iPSC-

TSC at passage 8), and Io et al.'s naïve hPSC-derived TSC (naïve cytotrophoblast or N-CT at passage 3-15); and 4) primary cytotrophoblast (CTB) (CTB-1E include our preps from 10 different 5-8 week-gestation placentae; other four samples include two 9-week and two 11-week gestation CTB preps from Io et al.). For hPSC lines, each dot represents a sample from an independent experiment (n = 2 for H1 and iPSC, day 0 and TSC, and all samples from Io et al.; n = 3 for all H9 samples); for CTB samples, each dot represents a biological replicate. Clusters from K-means clustering shown in grey dashed circles. **B)** Dendrogram of the same samples, showing primed and naïve hPSC and their early derivatives clustering separately (left) from primary CTB, hPSC-derived TSC (naïve and primed), as well as hPSC-derived TE (naïve and primed). **C)** Single cell RNAseq analysis of H9-ESC at day 0, at 12-hours, 24-hours and 4 days post-BMP4/IWP2 treatment, as well as H9-TSC, separated into 4 clusters by Seurat. Feature plots of pluripotency-, TE-, and CTB-associated markers show induction of TE- (and not naïve pluripotency-) associated genes, prior to finally transitioning into TSC state, with expression of CTB-associated markers. **D)** Ucell analysis using epiblast (EPI) and TE-specific genes from single cell RNAseq of extended culture human embryo dataset by Zhou et al., 2019. Note clusters 0 (H9-12h and 24h) and 1 (undifferentiated H9) are enriched in EPI genes, while clusters 2 (H9-TSC) and 3 (H9 at 4 days post-BMP4/IWP2 treatment) are enriched in TE genes. **E)** Analysis by PlacentaCellEnrich tool of transcriptomic signatures of BMP4/IWP2-treated hPSC, primary TSC, and hPSC-derived TSC, compared to undifferentiated hPSCs. Note similar enrichment proportions for syncytiotrophoblast (STB)-, extravillous trophoblast (EVT)-, and cytotrophoblast (CTB)-associated genes across all 3 comparisons. See also **Figure S4**.

Figure-1

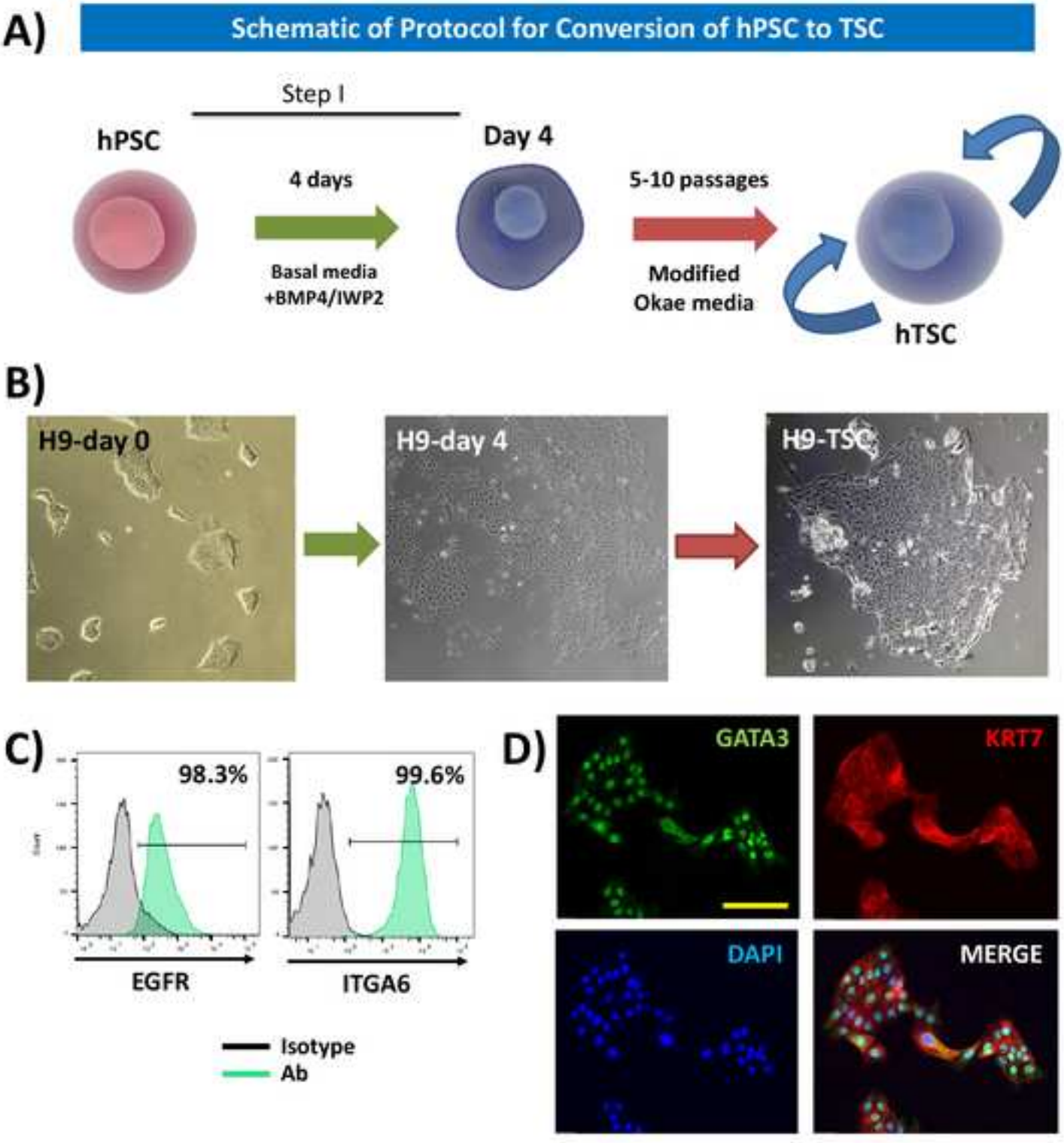

Figure-2

Click here to access/download;Figure;Figure-2.tif

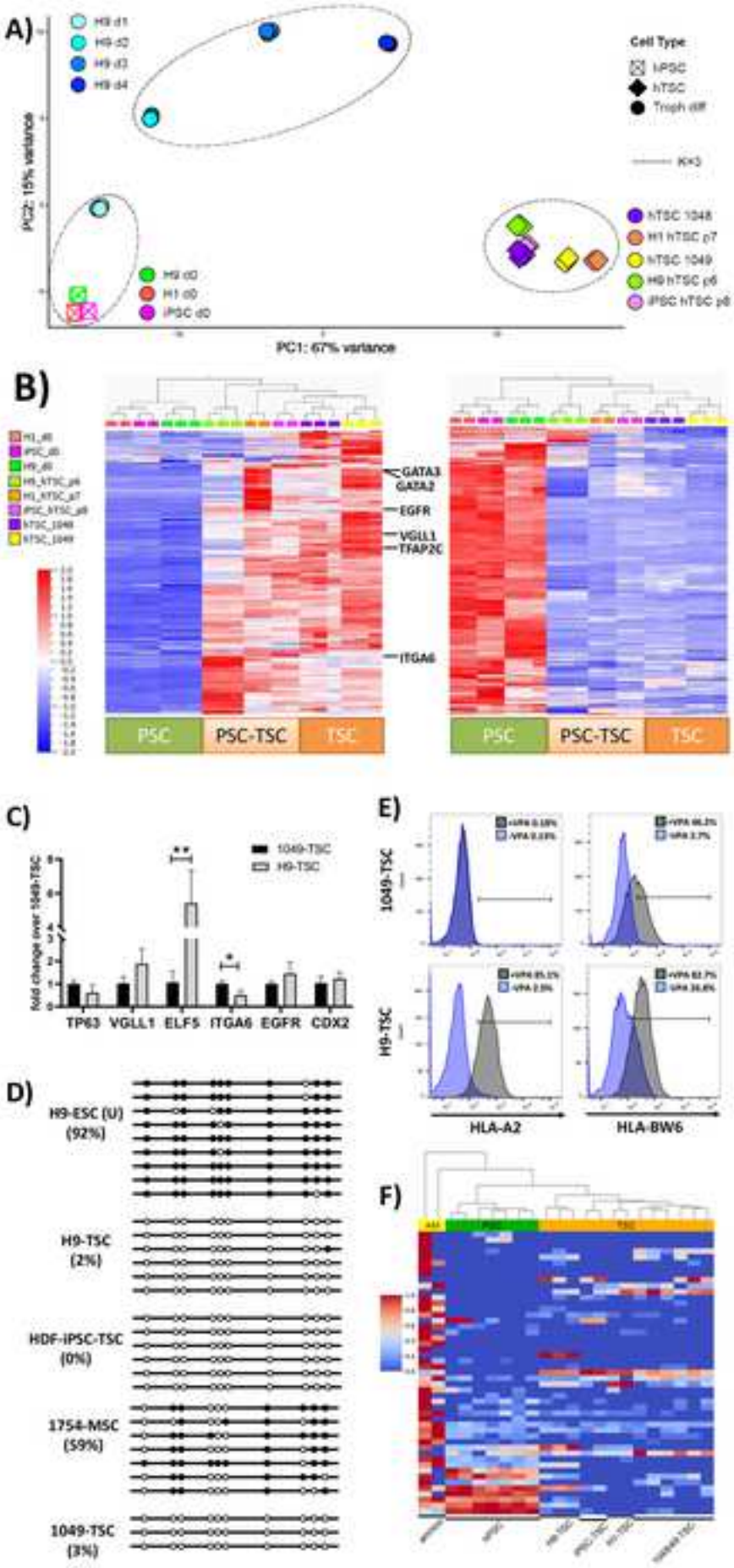

Figure-3

Click here to access/download;Figure;Figure-3.tif

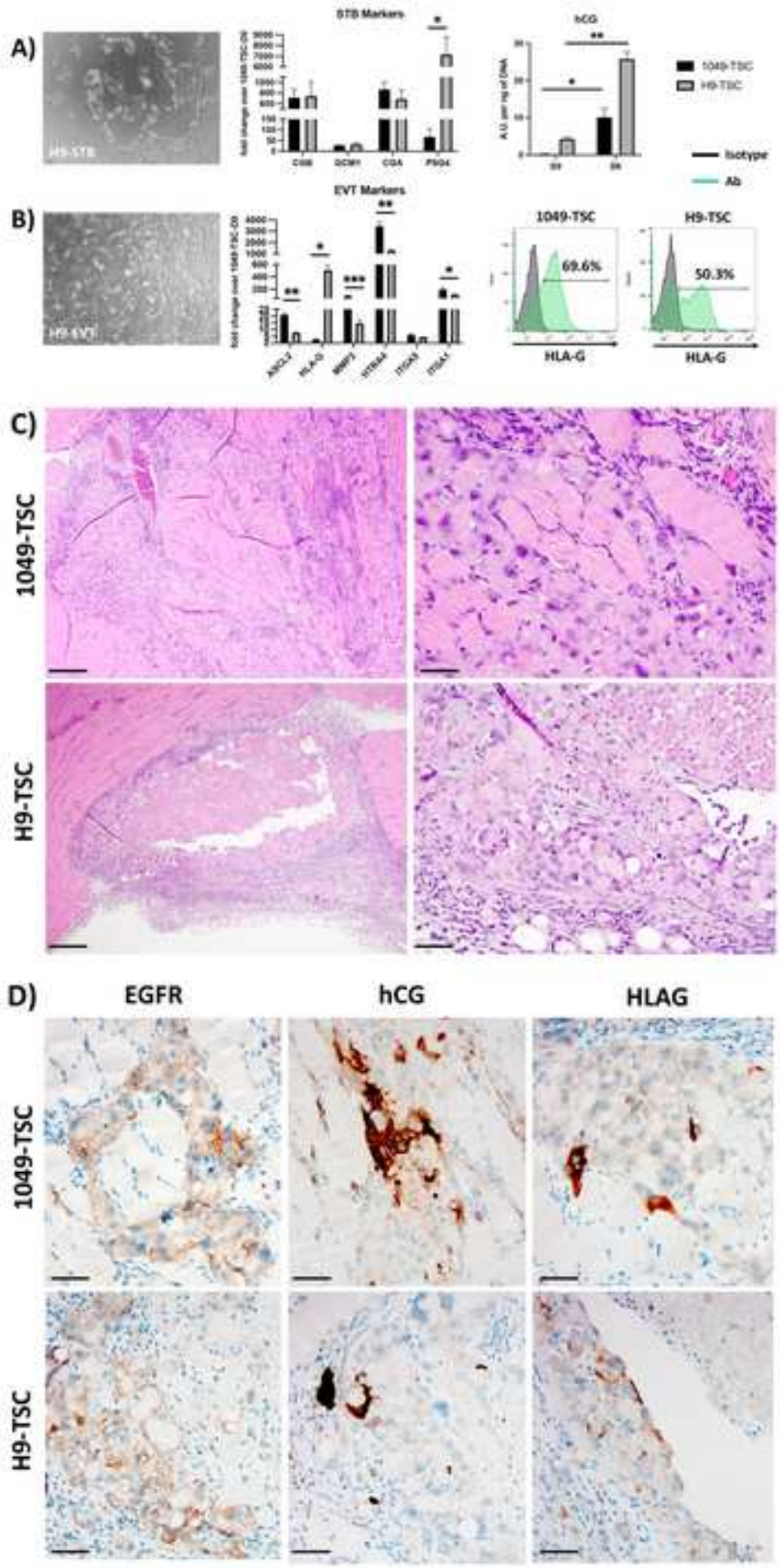

Figure-4

Click here to access/download;Figure;Figure-4.tif

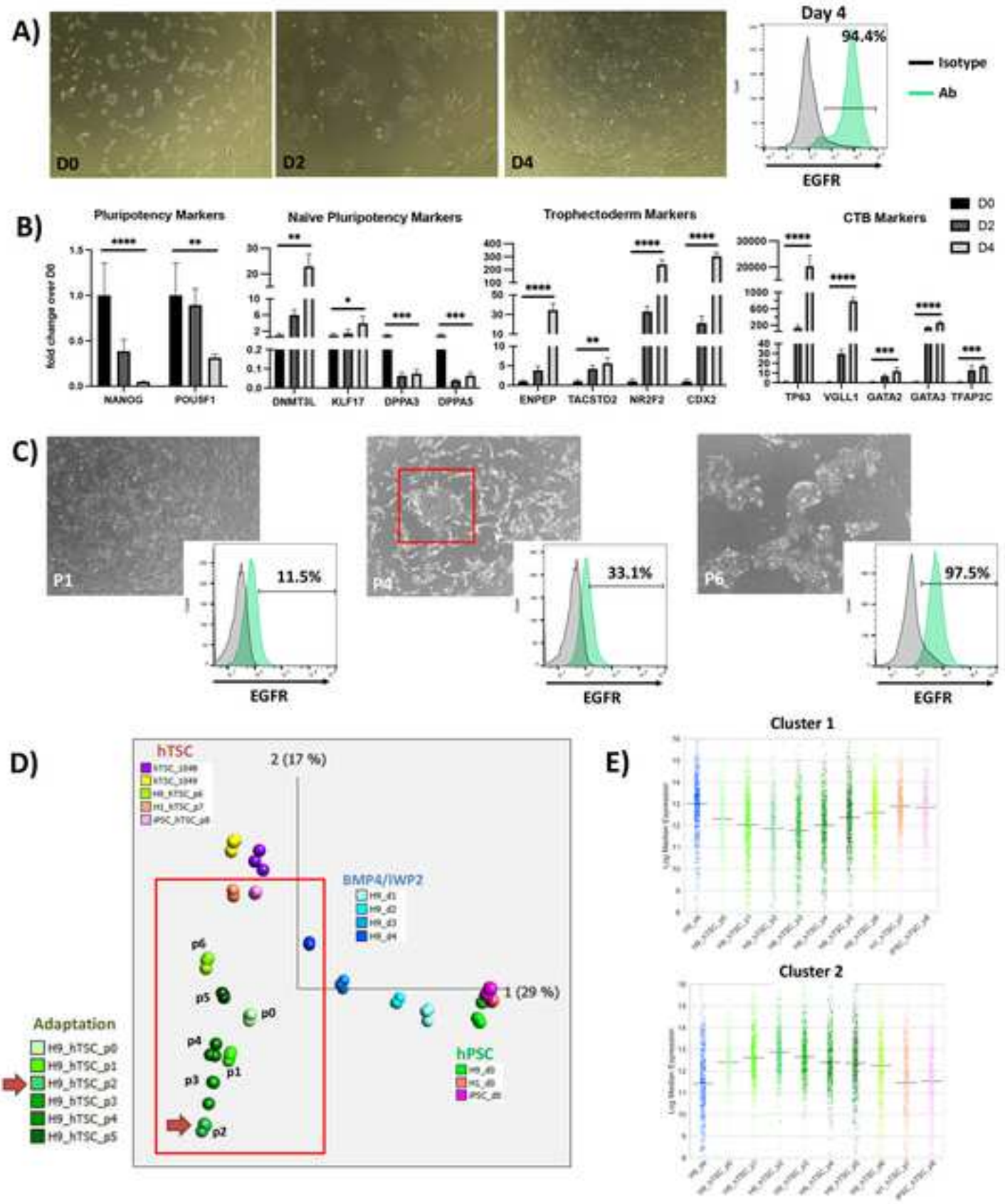

Figure-5

Click here to access/download;Figure;Figure-5.tif

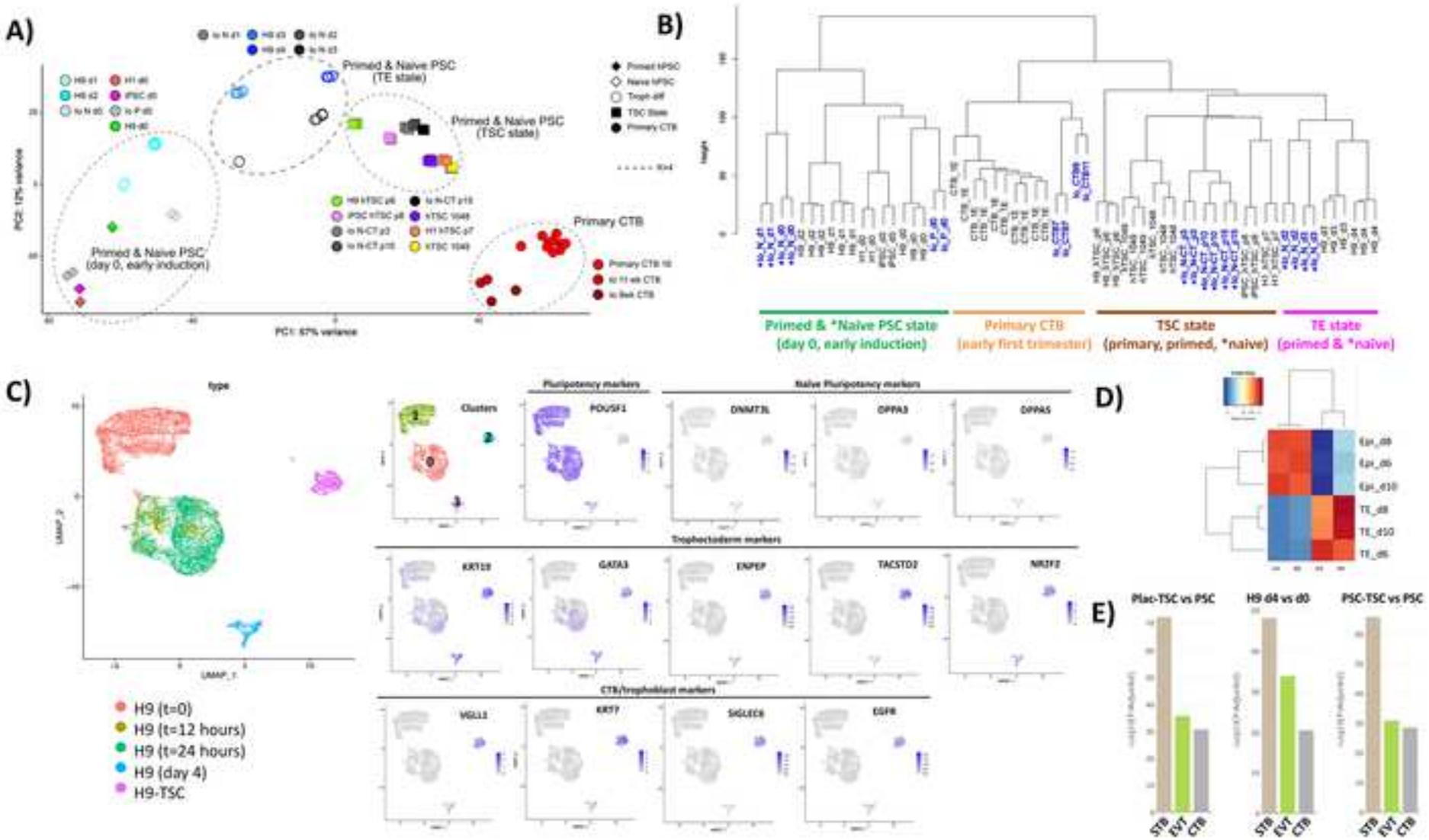

Supplemental Items

Figure S1. Derivation of trophoblast stem cells (TSC) from primed human pluripotent stem cells (hPSC) (related to **Figure 1**). **A)** Immunofluorescence staining of primary hTSC (1049 line) for GATA3 and KRT7, for comparison to hPSC-derived TSC (as shown in Figure 1D). Bar=124.5 µm. Data are representative of n = 3 independent experiments. **B)** Conversion of two additional primed hPSC lines (human dermal fibroblast/HDF-derived iPSC and H1-ESC) into TSC, expressing both EGFR and ITGA6. Data are representative of 2 independent experiments per line.

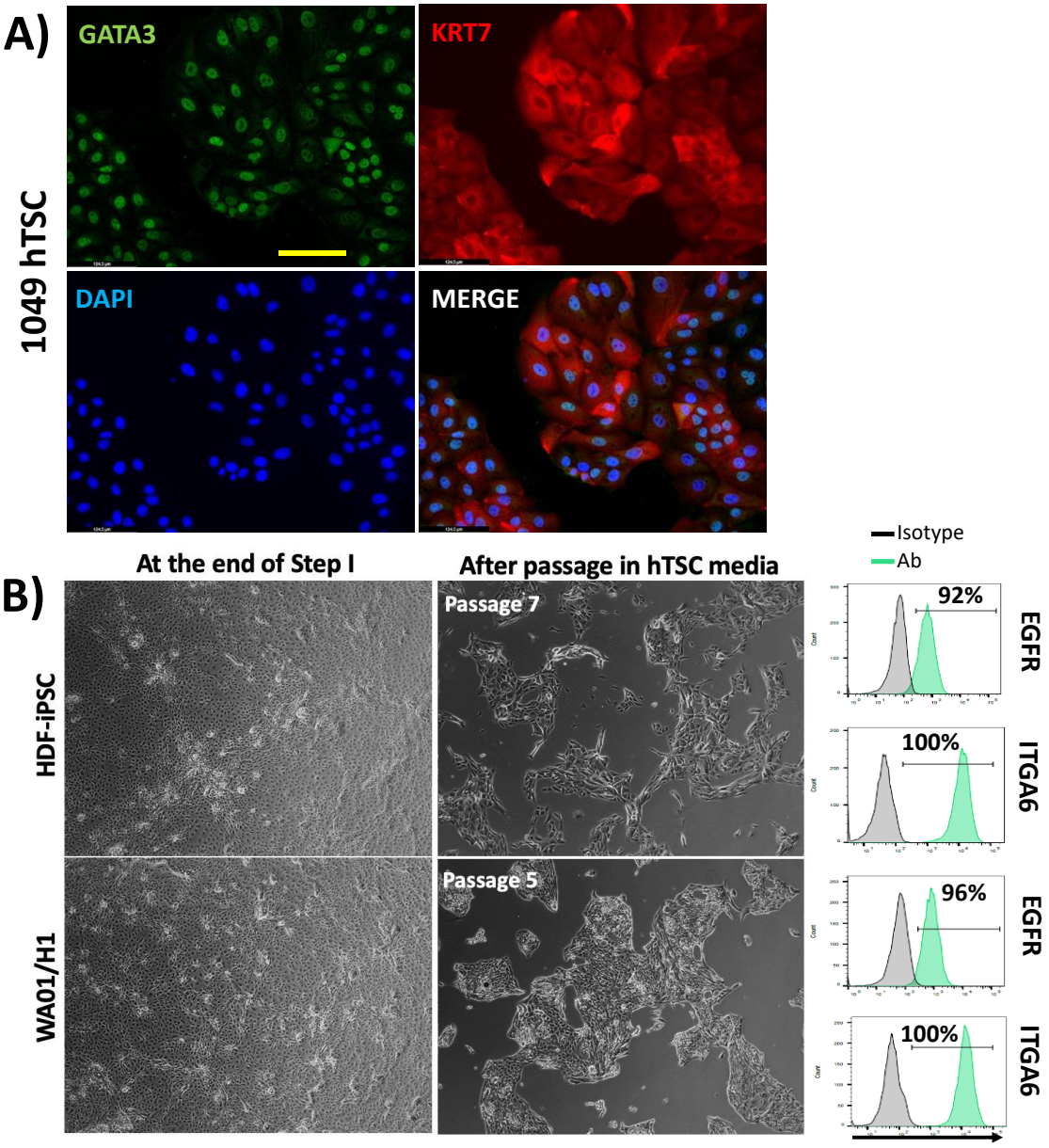

Figure S2. Comparison of hPSC-derived TSC to primary TSC and CTB (related to **Figure 2**). **A)** Primary hTSC (1049) and H9-TSC co-stained for TP63/CDH1 and OCT4/F-actin (phalloidin); Bar=124.5 µm. **B)** Primary hTSC (1049), H9 following 4 days of BMP4/IWP2 treatment, and H9-TSC, co-stained for CDX2 and TP63; Bar=124.5 µm. **C)** Principal component analysis of undifferentiated hPSC, hPSC after 1-4 days of BMP4/IWP2 treatment, and primary and hPSC-derived TSC, in comparison to CTB isolated from early (5-8 weeks) or late (10-14 weeks) first trimester placentae. For hPSC lines, each dot represents a sample from an independent experiment (n = 2 for H1 and iPSC, day 0 and TSC; n = 3 for all H9 samples); for CTB samples, each dot represents a biological replicate. **D)** Hierarchical clustering dendrograms of the same cells as in "C" compared to early- and late- first trimester CTB, either together or independently. Arrow points to the branch to which both primary and hPSC-derived TSC belong in each comparison. **E)** Expression of four miRNA members of the C19MC family in hPSC-derived hTSC (derived from H9 and HDF-iPSC), as compared to undifferentiated H9, primary hTSC (1049), and JEG3 trophoblast cell line by qPCR. Data were normalized to housekeeping miRNA gene, and shown as fold change over undifferentiated H9, and represent mean +/- SD for n = 3 independent experiments. **p<0.01, ****p<0.0001 by student's t-test.

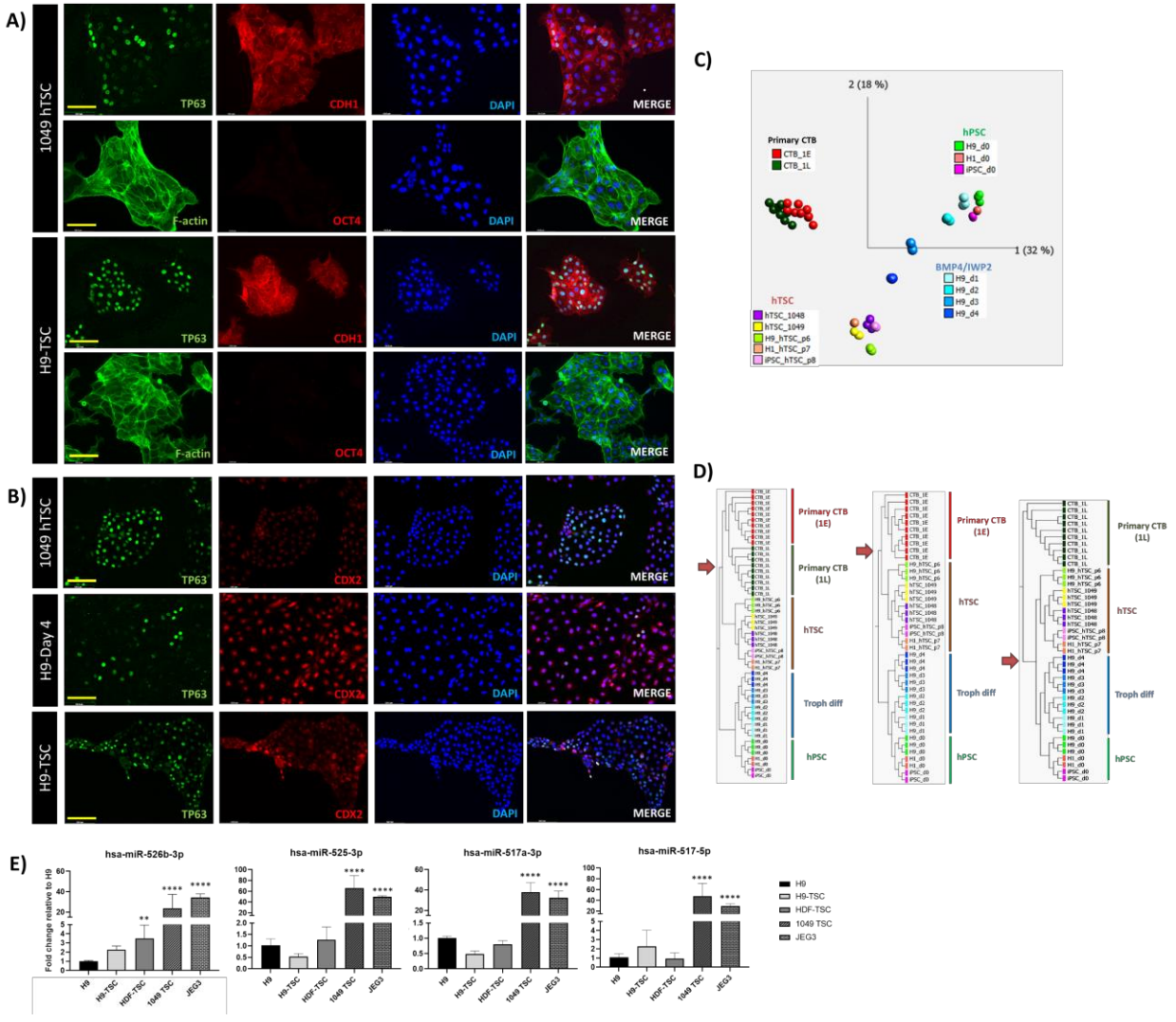

Figure S3. Analysis of gene expression changes during adaptation of BMP4/IWP2-treated hPSC in modified Okae TSC media (related to **Figure 4**). **A)** Proportion of genes (839), differentially up-regulated in primary TSC compared to undifferentiated hPSC, first decreases from 37% at 4 days of BMP4/IWP2 treatment to 28% after two passages in the modified Okae media, but then increases to 59% in hPSC-derived TSC. **B)** The adaptation did not change the nature of the cells as the most significant tissue-specific signature of all the timepoints was associated with "placenta." **C)** Heatmap showing genes differentially expressed (ANOVA q=0.05, variance filter = 0.01) between samples within the H9 adaptation from p0 to p6, the H9-day-4, and terminally-adapted H1/HDF-TSC. The heatmap is ordered according to clusters identified using Click clustering with cluster 1 containing genes showing initial downregulation until p2 of adaptation followed by a subsequent progressive upregulation through p6. Cluster 2 shows the converse pattern of gene expression, with a peak at p2 and subsequent downregulation through p6. **D)** GO pathway analysis (Hallmark Pathways MSigDB) of genes found in Cluster 1 (Top Table, see part **(C)**) and Cluster 2 (Bottom Table, see part **(C)**). Tables show the top 10 terms sorted by combined score.

A)

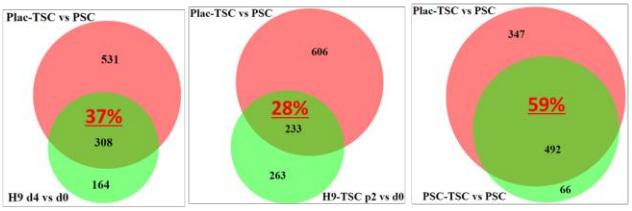

B)

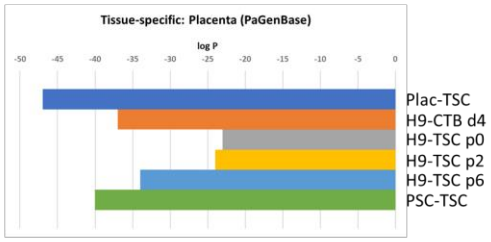

C)

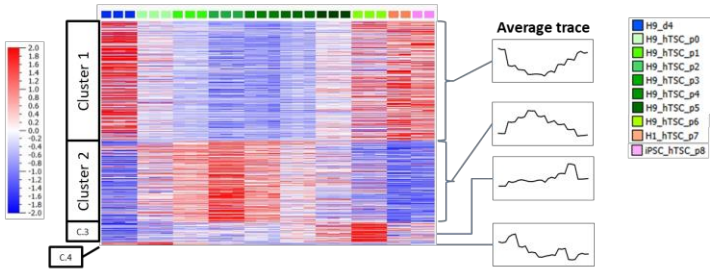

D)

	Index	Term	P-value	Adjusted P-value	Odds Ratio	Combined Score
Cluster 1	1	Myc Targets V1	5.74E-51	2.87E-49	16.80	1943.16
	2	mTORC1 Signaling	1.14E-24	2.85E-23	8.89	490.25
	3	Cholesterol Homeostasis	2.66E-13	3.33E-12	10.97	317.52
	4	G2-M Checkpoint	8.13E-16	1.35E-14	6.39	222.09
	5	UV Response Up	4.67E-13	4.67E-12	6.43	182.60
	6	Androgen Response	7.87E-10	4.37E-09	6.92	145.17
	7	Fatty Acid Metabolism	6.03E-10	4.37E-09	5.31	112.80
	8	Hypoxia	7.77E-10	4.37E-09	4.64	97.38
	9	Apical Junction	7.77E-10	4.37E-09	4.64	97.38
	10	Peroxisome	6.39E-08	2.13E-07	5.75	95.24

	Index	Term	P-value	Adjusted P-value	Odds Ratio	Combined Score
Cluster 2	1	Epithelial Mesenchymal Transition	4.94E-39	2.32E-37	16.52	1456.80
	2	Angiogenesis	4.83E-09	7.57E-08	16.95	324.54
	3	UV Response Dn	2.09E-15	4.92E-14	9.54	322.33
	4	Hedgehog Signaling	1.13E-06	1.06E-05	12.53	171.62
	5	Apical Junction	7.44E-07	8.74E-06	4.40	62.13
	6	Myogenesis	1.38E-05	1.08E-04	3.85	43.12
	7	Mitotic Spindle	1.86E-04	1.15E-03	3.34	28.66
	8	Apoptosis	3.13E-04	1.64E-03	3.54	28.58
	9	Hypoxia	1.96E-04	1.15E-03	3.32	28.33
	10	Protein Secretion	1.52E-03	5.94E-03	3.98	25.81

Figure S4. Principal component analysis of TE- and TSC-like cells derived from naïve and primed hPSC (related to **Figure 5**). Scatterplot shows analysis of our cells, combined with those published from Io et al. (Io et al., 2021), Wei et al. (Wei et al., 2021), and Liu et al (Liu et al., 2020). K-means clustering (K=4) shows from right to left: **A)** primary cytotrophoblast (CTB) (CTB-1E include our preps from 10 different 5-8 week-gestation placentae; an additional four samples included two 9-week and two 11-week gestation CTB preps from Io et al.); **B)** primary hTSC (our 1048 and 1049, and Wei et al.'s), naïve hPSC-derived TSC (Io et al. and Liu et al.), and primed hPSC-derived TSC (our H9-, H1-, iPSC-derived TSC, and Wei et al.'s); **C)** undifferentiated naïve hPSC (Io and Liu et al.) and early naïve trophoblast derivatives (Io naïve day 1, 2, and 3) and late primed trophoblast derivatives (H9 day 3 and 4 post-BMP4/IWP2 treatment); **D)** undifferentiated primed hPSC (day 0) and early primed trophoblast derivatives (H9, day 1 and 2 post-BMP4/IWP2 treatment). Clusters from K-means clustering are shown in grey dashed circles and increasing K to 5 is shown in purple highlighted region of cluster "**C**." For hPSC lines, each dot represents a sample from an independent experiment; for CTB samples, each dot represents a biological replicate.

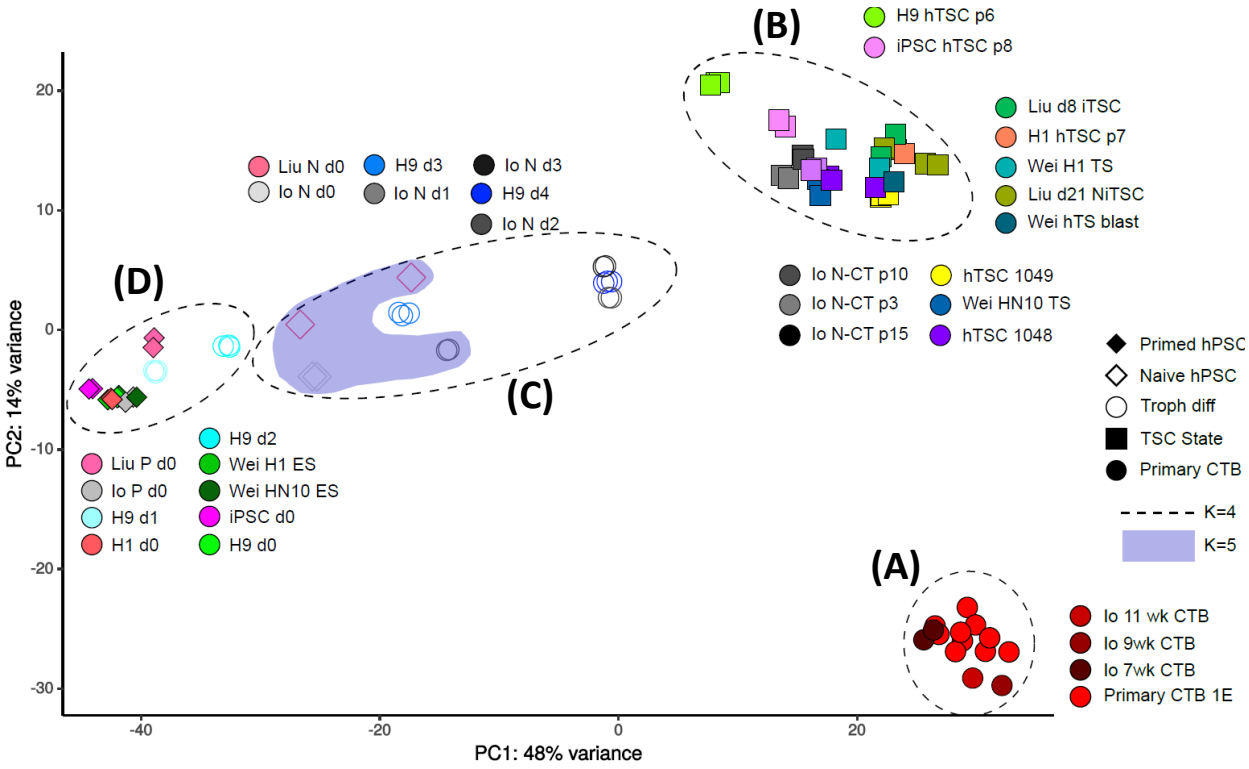

Supplemental Data Files.

Supplemental Data S1. Differentially expressed genes between primary TSC and primed hPSC-derived TSC (related to **Figure 2B** and **Figure S3A**).

Supplemental Data S2. Differentially expressed gene lists from primed H9 cells during adaptation to hTSC media (related to **Figure S3A-B**).

Supplemental Data S3. GO pathway analysis (Hallmark Pathways MSigDB) of genes downregulated at p0 of TSC-adaptation compared to H9-Day-4 (genes listed in **Supplemental Data S2**).

Supplemental Data S4. Differentially expressed genes from H9-Day-4, TSC media adaptation (p0-p6), and fully adapted hPSC-derived TSC (related to **Figure 4D-E** and **Figure S3C**).

Supplemental Data S5. TE and EPI-specific gene signature from Zhou et al.'s single cell RNAseq of extended culture human embryo (Day 6, 8 and 10; related to **Figure 5D**) (Zhou et al., 2019).

Supplemental Table 1. List of primers used for qPCR (related to supplemental experimental procedures).

Gene name	Primer pairs (5'- end to 3' - end)	Gene name	Primer pairs (5'- end to 3' - end)
ASCL2	F: CACTGCTGGCAAACGGAGAC R: AAAACTCCAGATAGTGGGGGC	ITGA1	F: CTGGACATAGTCATAGTGCTGGA R: ACCTGTGTCTGTTTAGGACCA
CGA	F: CAACCGCCCTGAACACATCC R: CAGCAAGTGGACTCTGAGGTG	ITGA5	F: GGCTTCAACTTAGACGCGGAG R: TGGCTGGTATTAGCCTTGGGT
CGB	F: ACCCTGGCTGTGGAGAAGG R: ATGGACTCGAAGCGCACA	ITGA6	F: GGCGGTGTTATGTCCTGAGTC R: AATCGCCCATCACAAAAGCTC
CDX2	F: TTCACTACAGTCGCTACATCACC R: TTGATTTTCCTCTCCTTTGCTC	KLF17	F: CTGCCTGAGCGTGGTATGAG R: TCATCCGGGAAGGAGTGAGA
DNMT3L	F: TTCTGGATGTTCGTGGACAA R: ACATCTGGGATGGTGACTGG	L19	F: AAAACAAGCGGATTCTCATGGA R: TGCGTGCTTCCTTGGTCTTAG
DPPA3	F: GTTACTGGGCGGAGTTCGTA R: TGAAGTGGCTTGGTGTCTTG	MMP2	F: CCAAGGAGAGCTGCAACCTG R: TGGGCTTGCGAGGGAAGAAG
DPPA5	F: TGAAAGATCCAGAGGTGTTC R: ACTGGTTCACTTCATCCAAG	NANOG	F: CCTATGCCTGTGATTTGTGG R: CTTTGGGACTGGTGGAAGAA
EGFR	F: CTAAGATCCCGTCCATCGCC R: GGAGCCCAGCACTTTGATCT	NR2F2	F: GCCATAGTCCTGTTCACCTCA R: AATCTCGTCGGCTGGTTG
ELF5	F: AGTCTGCACTGACATTTTCTCATC R: CAGAAGTCCTAGGGGCAGTC	POU5F1	F: TGGGCTCGAGAAGGATGTG R: GCATAGTCGCTGCTTGATCG
ENPEP	F: TCCCAAAGAATACGGAGCACT R: TCATGGGGACAGACTTCTCAA	PSG4	F: CCAGGGTAAAGCGACCCATT R: AGAATATTGTGCCCGTGGGT
GATA2	F: CCTGTAGTTCCTGCCCCTCT R: AGCTGCCGACTCCCAGA	TACSTD2	F: ACAACGATGGCCTCTACGAC R: AGTTCACGCACCAGCACAC
GATA3	F: AGGGACGTCCTGTGCGAACT R: GGTCTGGATGCCTTCCTTCTTCAT	TFAP2C	F: GAAGAGGACTGCGAGGATCG R: GCTGATATTCGGCGACTCCA
HLAG	F: ACTGAGTGGCAAGTCCCTTT R: TGGGGAAGGAATGCAGTTCAG	TP63	F: CTGGAAAACAATGCCCAGA R: AGAGAGCATCGAAGGTGGAG
HTRA4	F: AAAGAACTGGGGATGAAGGAT R: TGACGCCAATCACATCACCAT	VGLL1	F: CTCCCGGCTCAGTTCACTATAA R: CCCAGTGGTTTGGTGGTGTA

Supplemental Experimental Procedures

Isolation of primary cytotrophoblast and derivation of human trophoblast stem cells and mesenchymal stem cells

Human placental tissues were collected under a UCSD Human Research Protections Program Committee Institutional Review Board-approved protocol; all patients provided informed consent for collection and use of these tissues. Primary cytotrophoblast (CTB) were isolated from a total of 10 early first trimester (gestational age range of 5 to 7 weeks) and 10 late first trimester (gestational age range of 10 to 14 weeks) normal placentae, defined as those coming from patients undergoing elective termination of pregnancy in the absence of known structural fetal abnormalities. CTB isolation was performed as previously described (Morey et al., 2021; Wakeland et al., 2017). Briefly, chorionic villi were minced, washed in Hanks' balanced salt solution (Gibco) and digested three times with DNase I (Roche) and trypsin (Gibco). The cells were then pelleted and separated on a Percoll gradient (Sigma-Aldrich) and subjected to sequential magnetic activated cell sorting (MACS) selection (Miltenyi Biotec). Specifically, cells were first subjected to negative selection using a PE-conjugated antibody against HLA-G (EXBIO MEM-G/9) to remove extravillous trophoblast (EVT). The unbound fraction was collected and CTB were selected using APC-conjugated antibody against EGFR (Biolegend #352906) and tested for purity using flow cytometry. CTB preparations yielding greater than 90% EGFR positivity were considered adequate and used in downstream experiments.

Human trophoblast stem cell (hTSC) lines were derived from early first trimester placentae as previously described (Morey et al., 2021). Cells were plated on collagen IV coated 12-well plates at a density of 200k cells per well and cultured in the same media used for culture of pluripotent stem cell-derived TSC (described below). Human mesenchymal stem cells (MSC) were isolated from umbilical cord (UC) tissues as previously described (Horii et al., 2021).

Human pluripotent stem cell culture and differentiation into TE-like cells

Trophoblast differentiation of human pluripotent stem cells was performed under a protocol approved by the UCSD Institutional Review Board and Embryonic Stem Cell Research Oversight Committee. Two human embryonic stem cell (hESC) lines (WA01/H1 and WA09/H9, obtained from WiCell Institute, Madison, WI, USA), and one iPSC line (reprogrammed from human dermal fibroblast/HDF from ScienCell Research Laboratories, using CytoTune-iPSC 2.0 Sendai Reprogramming Kit from ThermoFisher) (Touboul et al., 2016) were used in this study.

Prior to differentiation, hPSCs were converted to feeder-free conditions in StemFlex (ThermoFisher) on Geltrex- (ThermoFisher) coated plates (using 1:200 diluted Geltrex). Differentiation into trophectoderm (TE)-like cells was performed using the first step of the two-step trophoblast differentiation previously established in our lab (detailed in Horii et al. 2021). In brief, hPSCs were dissociated using TrypLE Express (ThermoFisher) and plated onto Geltrex coated plates in StemFlex in the presence of 5μM Y-27632 (Selleck Chemicals). The next day media was changed to first-step differentiation media: DMEM/F12 (ThermoFisher), with 1x ITS (Millipore-Sigma), 64μg/ml L-ascorbic acid (Millipore-Sigma), 543μg/ml NaHCO3 (Fisher Scientific), 2% BSA (Gemini), 10 ng/mL BMP4 (ThermoFisher), and 2μM IWP2 (Selleck Chemicals). Media was changed every day for 4 days. Conversion into TE-like cells was confirmed based on surface EGFR expression of over 90% by flow cytometry.

Flow cytometric analysis

Flow cytometry was conducted using live cells. Cells were collected and incubated at room temperature for one hour in 200μL FC buffer (1% BSA,10% FBS in PBS) with 1μg APC-conjugated mouse anti-human EGFR antibody (clone AY13, BioLegend) and 2μg PE-conjugated mouse anti-HLA-G antibody (MEM-G/9, ExBio) in combination, or 0.125μg APC-conjugated mouse anti-HLA-A2 (clone BB7.2, BD Pharmigen), 0.22μg PE-conjugated mouse anti-HLA-Bw6 (clone REA143, Miltenyi Biotec), and 0.5μg PE-conjugated rat IgG2b anti- CD49f (ITGA6, clone GoH3, BioLegend) as single antibody stains. APC-conjugated mouse IgG (cloneMOPC-21, BioLegend), PE-conjugated mouse IgG (cloneMOPC-21, BioLegend), and PE-conjugated rat IgG2b (clone 141945, R&D Systems) were used at the same concentration as isotype IgG controls. Cells were washed 3 times with Wash buffer (0.1% FBS in PBS) and analysis was carried out using a BD FACS-Canto Flow Cytometer.

In vitro differentiation of primary and hPSC-derived TSC

Differentiation into extravillous trophoblast (EVT) and syncytiotrophoblast (STB) was performed based on protocols slightly modified from Okae et al., 2018. Briefly, for EVT differentiation, TSCs were dissociated by using TrypLE Express and resuspended in complete EVT media, composed of DMEM/F12 no HEPES (ThermoFisher), 0.3% BSA (Gemini), 1x ITS-X (ThermoFisher), 100μM 2-mercaptoethanol (ThermoFisher), 2.5μM Y-27632 (Selleck Chemicals), 4% KSR (ThermoFisher), 7.5μM A83-01 (Tocris), 100ng/mL NRG1 (Abcam), and supplemented with 2% Matrigel (Corning). 200,000 cells were plated per well of a fibronectin- (MilliporeSigma, 20μg/mL) coated 6-well plate. On the 3rd day of differentiation, media was changed with EVT media without NRG1, and Matrigel was added to a final concentration of 0.5%. Differentiation was deemed complete on day 6 and cells were collected for analysis. For STB differentiation, TSCs were plated at 30% confluence. At this point, media was switched to STB differentiation media, composed of DMEM/F12 no HEPES (ThermoFisher), 0.3% BSA (Gemini), 1x ITS-X (ThermoFisher), 100μM 2-mercaptoethanol (ThermoFisher), 2.5μM Y-27632 (Selleck Chemicals), 4% KSR (ThermoFisher), 2μM Forskolin (Selleck Chemicals). Media was replaced at day 3, and differentiation was deemed complete on day 6 and cells were collected for analysis.

In vivo differentiation of primary and hPSC-derived TSC (tumor formation assay)

Use of mice for these assays was approved by the Institutional Animal Care and Use Committee (IACUC) at UC San Diego. Primary and hPSC-derived TSCs were grown to 90% confluence in TSC medium (as described above) and dissociated with TrypLE. 1.5 x 10^7 cells were resuspended in 0.15 mL of a 1:2 mixture of Matrigel and TSC medium, and subcutaneously injected into the flank or hindleg of 8-12-week-old male NOD-SCID mice (JAX Stock No: 005557). Tumor growths were collected 7-10 days after injection. The tumors were fixed in 10% neutral-buffered formalin overnight at 4°C, then processed and embedded in paraffin. H&E staining and IHC were performed on 5-μm sections of these tissues. IHC was performed on a Ventana Discovery Ultra automated stainer (Ventana Medical Systems) at the UC San Diego Advanced Tissue Technology Core lab. Following standard antigen retrieval, performed for 40 min at 95°C as per the manufacturer's protocol (Ventana Medical Systems), the sections were stained using mouse anti-HLAG antibody (1:6000; clone 4H84; Abcam), mouse anti-hCG antibody (1:75; clone #5H4-E2; Abcam), or mouse anti-EGFR antibody (1:15; clone 5B7; Ventana Medical Systems). Staining was visualized using 3,3′-diaminobenzidine (DAB, Ventana Medical Systems) and slides were counterstained with Hematoxylin. Slides were analyzed by conventional light microscopy on an Olympus BX43 microscope.

hCG hormone secretion assays

Cell culture supernatants were collected and stored at -80°C until use. Levels of total hCG were quantified using the hCG ELISA Kit (HC251F, Calbiotech Inc.) following manufacturer's protocol. Briefly, 100 μL of each diluted sample was incubated in the provided plate for 60min at room temperature. Samples were removed and wells were washed 3 times with 300uL 1x Wash Buffer. 100uL of TMB substrate was added to each well and incubated at room temperature for 15min. 50uL of stop solution was added to each well. Absorbance was immediately measured at 450nm using Tecan infinite 200Pro. The concentration (mIU/mL) was calculated based off of the standards provided. The concentrations were normalized to total DNA content, extracted by DNeasy (Qiagen), and quantified by NanoDrop spectrophotometer (ThermoFisher).

Immunofluorescence staining

Cultured cells were fixed in ice-cold 4% paraformaldehyde in phosphate-buffered saline for 10 minutes. Cells were then washed using PBS and blocked with a buffer consisting of 10% normal goat serum (Jackson Labs), 5% BSA (VWR), and 0.25% Triton-X in PBS for one hour. Cells were stained with the following primary antibodies in blocking buffer overnight at 4ºC: mouse anti-GATA3 antibody (ThermoFisher), mouse anti-p40 (delta-N isoform of TP63) antibody (Biocare Medical), rabbit anti-KRT7 antibody (Abcam), rabbit anti-CDH1 antibody (Cell Signaling Technology), rabbit anti-CDX2 antibody (Abcam). Cells were washed and incubated with Alexa 488- or Alexa 647-conjugated goat anti-mouse and goat anti-rabbit secondary antibodies for one hour at room temperature in the dark. Some cells were also stained using Alexa 488-conjugated phalloidin (Invitrogen). All cells were counterstained with DAPI (Invitrogen), then visualized using a Leica DM IRE2 inverted fluorescence microscope.

RNA isolation, cDNA preparation, and quantitative real-time PCR

Total RNA was isolated using NucleoSpin isolation Kit (Macherey-Nagel). RNA concentration was measured using Nanodrop. cDNA was prepared from total RNA using the Primescipt RT-Kit (Takara bio). Quantitative real-time PCR (qPCR) was performed using TB GREEN (Takara bio) on a Quant-it Studio 5 thermocycler (ThermoFisher). The primer sequences used are listed in **Supplemental Table 1**. Relative expression of each transcript was calculated using $\Delta\Delta C_T$ method, normalized to L19 rRNA.

For the miRNA qPCR, RNA was isolated using mirVana kit (ThermoFisher), and RNA concentration was measured with the Qubit™ RNA BR Assay Kit (Thermo Fisher). TaqMan® Advanced miRNA cDNA Synthesis kit (ThermoFisher) was used for cDNA synthesis, and TaqMan™ Fast Advanced Master Mix (ThermoFisher) was used for qPCR reaction, following the manufacture's protocol. Probes used for the reactions were from TaqMan™ Advanced miRNA Assays (ThermoFisher), targeting miRNAs hsa-miR-517a-3p (479485_mir), hsa-miR-517-5p (478980_mir), hsa-miR-525-3p (478995_mir), hsa-miR-526b-3p (478996_mir), and housekeeping miRNA hsa-miR-103a-3p (478253_mir). The experiment was performed on a Quant-it Studio 5 thermocycler (ThermoFisher). 10µg of RNA was used for each reaction, and relative expression of each transcript was calculated using $\Delta\Delta C_T$ method, normalized to hsa-miR-103a-3p.

RNA sequencing and analysis

For RNAseq, total RNA was isolated using the mirVana kit (Thermo Fisher). RNA concentration was measured with the Qubit™ RNA BR Assay Kit (Thermo Fisher) and RNA integrity with the Agilent RNA 6000 Nano Kit on an Agilent 2100 Bioanalyzer (Agilent). Only samples with RIN above 7.5 were used. RNAseq libraries were prepared using the TruSeq Stranded Total RNA Sample preparation kit with Ribo-Zero Gold (Illumina) at the IGM Genomics Center, University of California, San Diego, La Jolla, CA. Libraries were pooled and sequenced on NovaSeq 6000 S1Flow Cell (Illumina) to an average depth of 28 million uniquely mapped reads. Quality control was performed using FastQC (v. 0.11.8) and multiQC (v. 1.6). Reads were mapped to GRCh38.p10 (GENCODE release 26) using STAR (v. 2.7.3a) (Dobin et al., 2013) and annotated using featureCounts (subread v.1.6.3, GENCODE release 26 primary assembly annotation) (Liao et al., 2014). The STAR parameters used were: --runMode alignReads --outSAMmode Full --outSAMattributes Standard --genomeLoad LoadAndKeep --clip3pAdapterSeq AGATCGGAAGAGC --clip3pAdapterMMp 1. The featureCounts parameters were: -s 2 -p -t exon -T 13 -g gene_id. Ensembl genes without at least three samples with 10 or more reads were removed from analysis. Normalization was performed using the R (v. 3.6.3) package DESeq2 (v. 1.28.1) (Love et al., 2014). BiomaRt (v. 2.42.1) was used to convert Ensembl gene ID's to HUGO gene names. Data visualization was done in R (v. 4.0.2) using the packages ggplot2 (v3.3.3) and pvclust (v.2.2-0), in python (v.3.6.11) using the package seaborn (0.11.0), Qlucore Omics Explorer (v3.6) (Qlucore AB, Lund, Sweden), and BioVenn (Hulsen et al., 2008). Differential expression analysis was performed in Qlucore Omics Explorer: first low expression genes were eliminated by variance (0.01-0.02) and then the two-sided two-group comparison (equivalent to a t-test) with q-value <0.05 was used to identify differentially expressed genes. Up and down-regulated genes were manually separated and analyzed in Enrichr (Kuleshov et al., 2016) for gene ontology using MSigDB Hallmark 2020 and PaGenBase enrichment, and for placental cell type using the PlacentaCellEnrich tool (Jain and Tuteja, 2021). Gene Set Enrichment Analysis (GSEA) was performed using fgsea (v.1.12) with custom gene lists created from primary-derived TSC vs. hPSC differential expression analysis for Figure 2B, and using amnion specific genes as identified by Seetheram et al. (manuscript co-submitted by our collaborators to Stem Cell Reports) for Figure 2F. RNA-seq data for Figure 5A and Supplementary Figure 4 were combined using only genes found in all datasets and using limma removeBatchEffect command. Click clustering was performed in Expander (v6) using default parameters. Hierarchical clustering was done using the R (v. 4.0.2) package pvclust (v.2.2-0) and Qlucore.

For single cell sequencing, a total of 11,259 cells across all timepoints were run on the 10X Genomics platform with the Chromium Next GEM Single Cell 3' kit, with libraries prepared according to the manufacturer's protocol (10X Genomics). Libraries were pooled, and sequenced on the Illumina NovaSeq 6000 sequencer to an average depth of 20K reads per cell. Raw fastq files were aligned and quantified with the CellRanger (v 6.0.1) count function with default parameters to the human reference genome (GRCh38-2020-A). The counts matrix was filtered to retain genes expressed in greater than 0.1% of the cells, cells that express greater than 200 unique genes, genes expressed in greater than 10 cells, less than 20% mitochondrial reads, greater than 5% ribosomal reads and those with less than 5% hemoglobin reads. The R package Seurat v4 (Hao et al., 2021) was used with default values for preprocessing, cell cycle scoring, normalization using scTransform regressing out variables for mitochondrial percentages and cell

cycle phase, identifying variable features, linear dimensional reduction, clustering and visualization. The FeaturePlot function was used to visualize gene expression of selected genes.

To compare our single cell RNAseq data to those from extended culture human embryos, the single cell RNA sequencing dataset from Zhou et al. (Zhou et al., 2019) was re-processed and independently analyzed. In brief, raw fastq files were trimmed for adapter sequences via cutadapt (v1.10) (Kechin et al., 2017), and mapped with STAR (2.5.2a) (Dobin et al., 2013). Samtools (Li et al., 2009) was used to process sam files, as well as to sort and remove PCR duplicates of bam files. Counts for each gene were quantified using the Subread package FeatureCounts using the gene level quantification in paired-end mode (release 1.5.2) (Liao et al., 2014), and annotated using the Ensembl GRCh38 genome. The R package Seurat v3 (Stuart et al., 2019) was used for single cell-specific processing and clustering, with feature cutoff values between 2000-9000, RNA counts <500,000, and percent mitochondrial contribution <10%, with default values for subsequent processing and normalization. The total dataset was partitioned by day (Day 6, Day 8, and Day 10), and clustered individually to identify embryonic cell types, which were confirmed based on the expression of well-known marker genes. The top 200 marker genes for each lineage (epiblast, primitive endoderm, and trophectoderm) were used for subsequent score mapping. These gene lists were defined as the tissue-specific gene expression signatures. We then used the R package UCell (Andreatta and Carmona, 2021) to score tissue-specific gene signatures in our single cell dataset, which is based on the Mann-Whitney U statistic. Each cell in the single cell dataset received a tissue-specific signature score. We summarized the average score across all cell types in a cluster for each tissue-specific gene signature in a heatmap.

DNA isolation and ELF5 promoter methylation analysis

Genomic DNA was isolated using the DNeasy Blood and Tissue Kit (Qiagen) and quantified using the Qubit dsDNA BR assay kit (ThermoFisher), 500 ng of DNA was then bisulfite converted using the EZ DNA Methylation-Lightning Kit (Zymo Research) as per instructions. Following bisulfite conversion, the upstream promoter region of the ELF5 start site was amplified using a nested PCR and primers as described previously (Lee et al., 2016).

Primer Set #1:
forward: 5'-GGAAATGATGGATATTGAATTTGA-3';
reverse: 5'-CAATAAAAATAAAAACACCTATAACC-3'
Primer Set #2:
forward: 5'-GAGGTTTTAATATTGGGTTTATAATG-3';
reverse: 5'-ATAAATAACACCTACAAACAAATCC-3'

The 20µl PCR reactions were carried out using 10µl KAPA HiFi HotStart Uracil+ ReadyMix (2X), 0.5µl of the forward and reverse primers, 8µl of water, and 1µl of converted DNA. PCR conditions for the first and second PCR were as follows: 95°C 10:00, 35x (95°C 30s, 45°C 30s, 72°C 30s), 72°C 7:00. 1µl of the reaction product from the first PCR was used in the second PCR. Following both the first and second PCR, the PCR products were purified using DNA Clean & Concentrator (Zymo Research) and run on the BioAnalyzer (Agilent) for quality control. 2µl of the purified PCR fragment was then A-tailed using 2µL of Taq polymerase 5X reaction buffer, 0.2µL of 50 mM $MgCl_2$, 0.2mM dATP, and 1U of Taq DNA polymerase (Qiagen) in a total reaction volume of 10µL, and incubated at 70°C for 30 min. The products of the A-tailing reaction were then purified using the DNA Clean and Concentrator kit (Zymo Research). The resulting DNA was ligated into the pGEM-T Easy Vector (Promega) according to the manufacturer's instructions using a 1:3 plasmid:insert molar ratio and incubated overnight at 4°C. The ligation reaction was then transformed into DH5α competent bacteria (NEB, Cat# C2987H) and plated on LB Agar Plates with Ampicillin, IPTG, and X-gal (Teknova, Cat# L1949) and incubated overnight at 37°C. The plasmid DNA was then purified using the QIAprep Spin Miniprep Kit (Qiagen) and sent to Eton Bioscience Inc. for sequencing. The sequences were subsequently aligned and analyzed using the BiQAnalyzer software (Lutsik et al., 2011).

Supplemental References

Andreatta, M., and Carmona, S.J. (2021). UCell: Robust and scalable single-cell gene signature scoring. Comput. Struct. Biotechnol. J. *19*, 3796–3798.

Dobin, A., Davis, C.A., Schlesinger, F., Drenkow, J., Zaleski, C., Jha, S., Batut, P., Chaisson, M., and Gingeras, T.R. (2013). STAR: ultrafast universal RNA-seq aligner. Bioinformatics *29*, 15–21.

Hao, Y., Hao, S., Andersen-Nissen, E., Mauck, W.M., Zheng, S., Butler, A., Lee, M.J., Wilk, A.J., Darby, C., Zager, M., et al. (2021). Integrated analysis of multimodal single-cell data. Cell *184*, 3573-3587.e29.

Horii, M., Morey, R., Bui, T., Touma, O., Nelson, K.K., Cho, H.Y., Rishik, H., Laurent, L.C., and Parast, M.M. (2021). Modeling preeclampsia using human induced pluripotent stem cells. Sci. Rep. *11*.

Hulsen, T., de Vlieg, J., and Alkema, W. (2008). BioVenn - a web application for the comparison and visualization of biological lists using area-proportional Venn diagrams. BMC Genomics *9*.

Io, S., Kabata, M., Iemura, Y., Semi, K., Morone, N., Minagawa, A., Wang, B., Okamoto, I., Nakamura, T., Kojima, Y., et al. (2021). Capturing human trophoblast development with naive pluripotent stem cells in vitro. Cell Stem Cell *28*, 1023-1039.e13.

Jain, A., and Tuteja, G. (2021). PlacentaCellEnrich: A tool to characterize gene sets using placenta cell-specific gene enrichment analysis. Placenta *103*, 164–171.

Kechin, A., Boyarskikh, U., Kel, A., and Filipenko, M. (2017). cutPrimers: A New Tool for Accurate Cutting of Primers from Reads of Targeted Next Generation Sequencing. J. Comput. Biol. *24*, 1138–1143.

Kuleshov, M. V., Jones, M.R., Rouillard, A.D., Fernandez, N.F., Duan, Q., Wang, Z., Koplev, S., Jenkins, S.L., Jagodnik, K.M., Lachmann, A., et al. (2016). Enrichr: a comprehensive gene set enrichment analysis web server 2016 update. Nucleic Acids Res. *44*, W90–W97.

Lee, C.Q.E., Gardner, L., Turco, M., Zhao, N., Murray, M.J., Coleman, N., Rossant, J., Hemberger, M., and Moffett, A. (2016). What Is Trophoblast? A Combination of Criteria Define Human First-Trimester Trophoblast. Stem Cell Reports *6*, 257–272.

Li, H., Handsaker, B., Wysoker, A., Fennell, T., Ruan, J., Homer, N., Marth, G., Abecasis, G., and Durbin, R. (2009). The Sequence Alignment/Map format and SAMtools. Bioinformatics *25*, 2078–2079.

Liao, Y., Smyth, G.K., and Shi, W. (2014). featureCounts: an efficient general purpose program for assigning sequence reads to genomic features. Bioinformatics *30*, 923–930.

Liu, X., Ouyang, J.F., Rossello, F.J., Tan, J.P., Davidson, K.C., Valdes, D.S., Schröder, J., Sun, Y.B.Y., Chen, J., Knaupp, A.S., et al. (2020). Reprogramming roadmap reveals route to human induced trophoblast stem cells. Nature *586*, 101–107.

Love, M.I., Huber, W., and Anders, S. (2014). Moderated estimation of fold change and dispersion for RNA-seq data with DESeq2. Genome Biol. *15*.

Lutsik, P., Feuerbach, L., Arand, J., Lengauer, T., Walter, J., and Bock, C. (2011). BiQ Analyzer HT: locus-specific analysis of DNA methylation by high-throughput bisulfite sequencing. Nucleic Acids Res. *39*.

Morey, R., Farah, O., Kallol, S., Requena, D.F., Meads, M., Moretto-Zita, M., Soncin, F., Laurent, L.C., and Parast, M.M. (2021). Transcriptomic Drivers of Differentiation, Maturation, and Polyploidy in Human Extravillous Trophoblast. Front. Cell Dev. Biol. *9*.

Okae, H., Toh, H., Sato, T., Hiura, H., Takahashi, S., Shirane, K., Kabayama, Y., Suyama, M., Sasaki, H., and Arima, T. (2018). Derivation of Human Trophoblast Stem Cells. Cell Stem Cell *22*, 50-63.e6.

Stuart, T., Butler, A., Hoffman, P., Hafemeister, C., Papalexi, E., Mauck, W.M., Hao, Y., Stoeckius, M., Smibert, P., and Satija, R. (2019). Comprehensive Integration of Single-Cell Data. Cell *177*, 1888-1902.e21.

Touboul, T., Chen, S., To, C.C., Mora-Castilla, S., Sabatini, K., Tukey, R.H., and Laurent, L.C. (2016). Stage-specific regulation of the WNT/β-catenin pathway enhances differentiation of hESCs into hepatocytes. J. Hepatol. *64*, 1315–1326.

Wakeland, A.K.A.K., Soncin, F., Moretto-Zita, M., Chang, C.-W.C.W., Horii, M., Pizzo, D., Nelson, K.K.K.K., Laurent, L.C.L.C., and Parast, M.M.M. (2017). Hypoxia Directs Human Extravillous Trophoblast Differentiation in a Hypoxia-Inducible Factor–Dependent Manner. Am. J. Pathol. *187*, 767–780.

Wei, Y., Wang, T., Ma, L., Zhang, Y., Zhao, Y., Lye, K., Xiao, L., Chen, C., Wang, Z., Ma, Y., et al. (2021). Efficient derivation of human trophoblast stem cells from primed pluripotent stem cells. Sci. Adv. *7*.

Zhou, F., Wang, R., Yuan, P., Ren, Y., Mao, Y., Li, R., Lian, Y., Li, J., Wen, L., Yan, L., et al. (2019). Reconstituting the transcriptome and DNA methylome landscapes of human implantation. Nature *572*, 660–664.

Click here to access/download

Supplemental Movies and Spreadsheets

Data_S2.csv

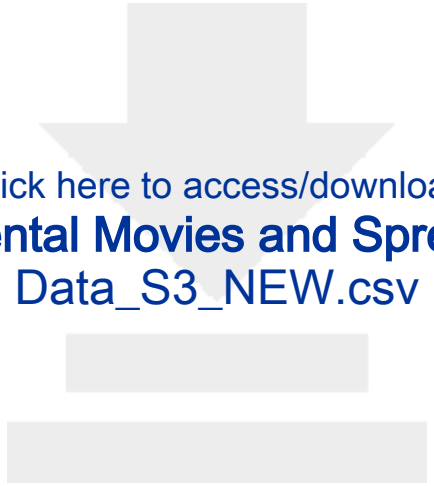

Click here to access/download

Supplemental Movies and Spreadsheets

Data_S3_NEW.csv

Click here to access/download

Supplemental Movies and Spreadsheets

Data_S4.csv

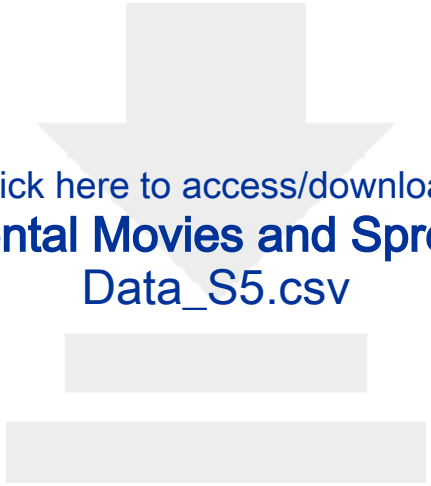

Click here to access/download

Supplemental Movies and Spreadsheets

Data_S5.csv